NASA TECHNICAL NOTE

AIRBORNE LASER-RADAR STUDIES OF THE LOWER ATMOSPHERE

by Samuel H. Melfi and Joseph W. Stickle

Langley Research Center

Langley Station, Hampton, Va.

1. Report No. NASA TN D-5558	2. Government Accession No.	3. Recipient's Catalog No.
4. Title and Subtitle AIRBORNE LASER-RADAR STUDIES OF THE LOWER ATMOSPHERE		5. Report Date December 1969
		6. Performing Organization Code
7. Author(s) Samuel H. Melfi and Joseph W. Stickle		8. Performing Organization Report No. L-5565
		10. Work Unit No. 126-61-04-05-23
9. Performing Organization Name and Address NASA Langley Research Center Hampton, Va. 23365		11. Contract or Grant No.
		13. Type of Report and Period Covered Technical Note
12. Sponsoring Agency Name and Address National Aeronautics and Space Administration Washington, D.C. 20546		
		14. Sponsoring Agency Code

15. Supplementary Notes

16. Abstract

In the present investigation a theoretical model of ruby-laser radiation backscatter with a wavelength of 0.6943 μm in the lower atmosphere has been developed. This model accounts for scattering from air molecules and atmospheric aerosols. Molecular scattering appears to predominate over aerosol scattering in the altitude range from 4 to 14 km. Above 14 km, an aerosol layer increases the scattering by approximately a factor of 2 above Rayleigh (molecular) predictions. An airborne laser system has been developed and flown from near sea level to an altitude of 11 km. The results of these airborne measurements agreed well with the model predictions.

This investigation was initiated to investigate the possible correlation between molecular or aerosol density fluctuations due to clear-air turbulence and laser-radar return from the atmosphere; however, no correlation was obtained. This result, however, does not preclude using laser backscatter systems as atmospheric probes, since the system used in the present investigation was extremely insensitive to the detection of molecular or aerosol density fluctuations. By using the results of this investigation and the theoretical model, an analysis of a general airborne laser system has been performed. This analysis has indicated that use of an improved system with better sensitivity and which is within the state of the art would make the airborne laser system a valuable tool for investigation of atmospheric phenomena associated with molecular and aerosol density changes.

17. Key Words Suggested by Author(s) Laser system Molecular and aerosol density Lower atmosphere	18. Distribution Statement Unclassified — Unlimited		
19. Security Classif. (of this report) Unclassified	20. Security Classif. (of this page) Unclassified	21. No. of Pages 56	22. Price* $3.00

*For sale by the Clearinghouse for Federal Scientific and Technical Information
Springfield, Virginia 22151

AIRBORNE LASER-RADAR STUDIES OF THE LOWER ATMOSPHERE

By Samuel H. Melfi and Joseph W. Stickle
Langley Research Center

SUMMARY

In the present investigation a theoretical model of ruby-laser radiation backscatter with a wavelength of 0.6943 μm in the lower atmosphere has been developed. This model accounts for scattering from air molecules and atmospheric aerosols. Molecular scattering appears to predominate over aerosol scattering in the altitude range from 4 to 14 km. Above 14 km, an aerosol layer increases the scattering by approximately a factor of 2 above Rayleigh (molecular) predictions. An airborne laser system has been developed and flown from near sea level to an altitude of 11 km. The results of these airborne measurements agreed well with the model predictions.

This investigation was initiated to investigate the possible correlation between molecular or aerosol density fluctuations due to clear-air turbulence and laser-radar return from the atmosphere; however, no correlation was obtained. This result, however, does not preclude using laser backscatter systems as atmospheric probes, since the system used in the present investigation was extremely insensitive to the detection of molecular or aerosol density fluctuations. By using the results of this investigation and the theoretical model, an analysis of a general airborne laser system has been performed. This analysis has indicated that use of an improved system with better sensitivity and which is within the state of the art would make the airborne laser system a valuable tool for investigation of atmospheric phenomena associated with molecular and aerosol density changes.

INTRODUCTION

Many investigations have been made on the scattering of light in the atmosphere. The first proposal for obtaining density profiles by measuring scattered light from a ground-based searchlight was made in 1930. (See ref. 1.) In 1937 (ref. 2), 1939 (ref. 3), and 1954 (ref. 4), molecular densities above 10 km were measured by using the technique of reference 1. More recently, with the advent of the high-powered ruby laser, light-scatter probing of the atmosphere has been extended to higher altitudes. It was reported in 1963 that atmospheric backscatter from a ruby laser had been measured up to an altitude of 140 km. (See ref. 5.) Subsequent investigations in which laser probing techniques

were used are reported in references 6 to 10. In reference 9 "ghost" returns from apparently clear air when using a ground-based ruby laser were observed. In reference 10 these ghost returns were attributed to scattering by layers of atmospheric aerosols. By using an airborne laser, an inconclusive correlation between laser returns and clear-air turbulence was found. (See ref. 11.)

Based primarily on the discoveries reported in references 9 and 10, a program was initiated at Langley Research Center to probe the atmosphere by using an airborne ruby laser. To evaluate the capability of a laser system to detect molecular and aerosol density gradients, a theoretical model of light scattering in the atmosphere is developed herein. The model is then verified by comparing it with experimental data obtained while flying a laser-equipped airplane at various altitudes from sea level to 11 km. With this verification, the model is used to determine the capabilities of laser systems in general and to predict the performance of an improved system that is well within the present state of the art.

SYMBOLS

A_r effective receiver area, meters^2

$A_T(R)$ transmitted beam cross-section area at location of scattering volume, meters^2

a change in aerosol density, percent

ΔB receiver bandwidth, hertz

$\left.\begin{array}{l} C(h) \\ C'(h) \end{array}\right\}$ constants of aerosol distribution at altitude h

c velocity of light, 3.00×10^8 meters-second^{-1}

D depolarization factor

E_T total energy transmitted by laser pulse, joules

F anisotropy factor

$f(\theta,\lambda)$ scattering function, steradian^{-1}-meter^{-1}

$f_M(h)$ Mie scattering function with $\theta = 180^O$ and $\lambda = 0.6943$ micrometer, steradian^{-1}-meter^{-1}

2

$f_M(\theta,\lambda,h)$ Mie scattering function, steradian^{-1}-meter^{-1}

$f_R(h)$ Rayleigh scattering function with $\theta = 180^O$ and $\lambda = 0.6943$ micrometer, steradian^{-1}-meter^{-1}

$f_R(\theta,\lambda,h)$ Rayleigh scattering function, steradian^{-1}-meter^{-1}

$f_t(h)$ total scattering function with $\theta = 180^O$ and $\lambda = 0.6943$ micrometer, steradian^{-1}-meter^{-1}

G gain of the photomultiplier

g nondimensional size parameter of atmospheric aerosols, $2\pi r/\lambda$

h altitude of airplane, meters

$\left.\begin{array}{l} i_1(\theta,\lambda,\iota,p) \\ i_2(\theta,\lambda,\iota,p) \end{array}\right\}$ Mie scattering amplitudes of scattered light perpendicular and parallel, respectively, to plane through direction of propagation of incident and scattered beams

$J_{A,D}$ anode dark current, amperes

K parametric variable

k wave number, $2\pi/\lambda$, micrometer^{-1}

m change in molecular density, percent

$N_{e,B}$ number of photoelectrons produced at photocathode of receiver by sky brightness in a counting time t_c, photoelectrons

$N_{e,D}$ number of thermal electrons (dark current) produced at photocathode of receiver in a counting time t_c, electrons

$N_{e,R}$ number of photoelectrons produced at photocathode of receiver by Rayleigh scattering in a counting time t_c, photoelectrons

$N_{e,t}$ number of photoelectrons produced at photocathode of receiver by Rayleigh and Mie scattering in a counting time t_c, photoelectrons

$N_M(h)$ — number of Mie scattering centers in scattering volume

$N_R(h)$ — number of Rayleigh scattering centers in scattering volume

n — number density, meter^{-3}

$n_M(h)$ — number density of Mie scattering centers at scattering volume, meter^{-3}

$n_M(r,h)$ — number density of Mie scattering centers with aerosol radius r at altitude h, meter^{-3}

$n_R(h)$ — number density of Rayleigh scattering centers at scattering volume, meter^{-3}

P_r — power incident on receiver, watts

P_T — average power transmitted by laser, watts

p — shape of aerosol particles

Q — receiver subsystem quality factor, $\eta\gamma A_r/\Delta B$, second-meter^2

R — range of the scattering volume in front of airplane, meters

r — radius of atmospheric aerosols, micrometers

S/N — signal-to-noise ratio

S_a/N — signal-to-noise ratio due to a change in aerosol density

S_m/N — signal-to-noise ratio due to a change in molecular density

s_r — sensitivity of receiver subsystem, volt-microwatt^{-1}

t_c — counting time of receiver, seconds

t_E — elapsed time as measured by receiver, microseconds

$V(t_E)$ — voltage at oscilloscope, volts

v — scattering volume, meters^3

4

w	pulse width, meters
$\bar{\alpha}$	average molecular polarizability of air up to $h = 80$ kilometers, meters^3
$\beta_M(h)$	extinction coefficient due to Mie scattering centers, meter^{-1}
$\beta_O(h)$	extinction coefficient due to ozone molecules, meter^{-1}
$\beta_R(h)$	extinction coefficient due to Rayleigh scattering centers, meter^{-1}
$\beta_t(h)$	total extinction coefficient, meter^{-1}
γ	receiver optical efficiency
δ_r	field of view of receiver, mrad
δ_T	beamwidth of laser transmitter, mrad
ζ	conversion factor from energy to photons at $\lambda = 0.6943$ micrometer, 3.51×10^{18} photons–joule^{-1}
η	receiver photocathode quantum efficiency, photoelectrons/photon
θ	scattering angle (measured between forward direction of incident beam and direction of observation), degrees or radians
ι	average index of refraction of the atmospheric aerosol
κ	curve constant of the atmospheric return, volts-second^2
λ	wavelength of incident light, micrometers
$\Delta\nu$	optical bandwidth of the receiver, micrometers
σ	standard deviation
$\sigma(\theta,\lambda)$	differential cross section, meters^2-steradian^{-1}
σ_M	Mie extinction cross section, meters^2

$\sigma_M(\theta,\lambda)$ differential Mie scattering cross section, $\text{meters}^2\text{-steradian}^{-1}$

$\sigma_R(\theta,\lambda)$ differential Rayleigh scattering cross section, $\text{meters}^2\text{-steradian}^{-1}$

τ width measured at half-power points of laser pulse, seconds

ϕ polar coordinate, degrees or radians

Ω_r solid angle subtended by the receiver, steradians

Subscript:

C   correction for attenuation effects in the atmosphere

THEORY

A diagram of the general airborne backscattering problem is shown in figure 1. Scattering of light in the atmosphere is produced by scattering by air molecules and atmospheric aerosols. Equation (1) gives a relationship between the power transmitted by the laser and the power incident on the receiver and is derived in appendix A:

$$P_r = \frac{cE_T A_r}{2R^2}\left[\sigma_R(\theta,\lambda)n_R(h) + \sigma_M(\theta,\lambda)n_M(h)\right]e^{-2\beta_t(h)R} \tag{1}$$

There exists a general relationship between the scattering function, the differential cross section, and the number density which is given by

$$f(\theta,\lambda) = \sigma(\theta,\lambda)n \tag{2}$$

By using this relationship, equation (1) reduces to

$$P_r = \frac{cE_T A_r}{2R^2}\left[f_R(\theta,\lambda,h) + f_M(\theta,\lambda,h)\right]e^{-2\beta_t(h)R} \tag{3}$$

Equation (3) indicates that scattering in the atmosphere can be analyzed by considering separately Rayleigh scattering (including molecules and aerosols with diameters much smaller than the incident wavelength) and Mie scattering (aerosols with diameters on the order of the incident wavelengths).

The scattering functions for Rayleigh scattering $f_R(h)$ and Mie scattering $f_M(h)$ have been derived in appendixes B and C, respectively, with $\theta = 180^O$ and $\lambda = 0.6943\ \mu m$ and by assuming a polydisperse collection of spherical aerosols as

$$\left.\begin{aligned} f_R(h) &= \left(2.10 \times 10^{-32}\right)n_R(h)\ \ sr^{-1}m^{-1}\\[10pt] f_M(h) &= \left(6.0 \times 10^{-9}\right)n_M(h)\ \ sr^{-1}m^{-1} \end{aligned}\right\} \tag{4}$$

These quantities are shown plotted as a function of altitude in figure 2. The molecular number density of the Rayleigh scattering function is a function of altitude, which can be obtained from reference 12. The aerosol number density of the Mie scattering function is developed in appendix D and given in table I. Atmospheric extinction coefficient $\beta_t(h)$ is presented in appendix E. The solid curve in figure 2 is the sum of the Rayleigh and Mie scattering functions. It represents the total scattering function for clear air as a function of altitude. This model predicts that backscatter light at a wavelength of 0.6943 μm in the altitude range from 4 to 14 km is primarily due to air molecules. Above 14 km, an aerosol layer increases the scattering by approximately a factor of 2 above Rayleigh predictions.

EXPERIMENTAL VERIFICATION OF THE MODEL

Description of the Airborne Laser System

A block diagram of the airborne laser system used to verify the theoretical model is shown in figure 3. This system can be conveniently divided into three subsystems: the transmitter subsystem, the receiver subsystem, and the display and recording subsystem. The location of the three subsystems is indicated on a photograph of the jet airplane used in this investigation. (See fig. 4.) Figures 5 and 6 are photographs of the equipment removed from the airplane.

The transmitter subsystem consists of a Q-switched ruby laser, collimating optics, and an output monitor. The characteristics of this subsystem are summarized in table II. Temperature control of the laser head by a closed-loop cooling system maintains the laser wavelength at 0.6943 μm. The output monitor detects the laser radiation as it passes through the collimating optics. The output of the monitor photodiode is used to trigger the oscilloscope in the display and recording subsystem and is also electrically integrated to provide a measure of the energy in each laser pulse.

The receiver subsystem consists of receiving optics, a temperature-controlled interference filter, and a photomultiplier tube. The characteristics of the receiver subsystem are summarized in table II. The display and recording subsystem consists of an oscilloscope and 35-millimeter camera. The oscilloscope has a bandwidth of 50 MHz,

which is the limiting bandwidth of the system, with a two-channel input. The camera has an automatic film advance which is capable of framing at 1 frame/sec.

Calibration and Alinement

The transmitter and receiver were calibrated before and after each flight, and their optical axes were alined periodically during the series of experiments.

The laser transmitter was calibrated by using a thermopile calorimeter. Prior to the 28th flight test, the output power used in reducing the data was assumed to be an average of the pre- and post-flight calorimeter measurements. Beginning with flight 28, a photodiode was utilized to record the output of individual pulses during a flight. The photodiode was calibrated by firing the laser into the calorimeter a number of times (10 to 20) and recording the output of the calorimeter along with the integrated output of the photodiode. These data were plotted. A straight-line fit to the data was made which gave a constant relating total energy output of the laser to maximum deflection on the oscilloscope of the integrated output of the photodiode. This output of the photodiode was recorded with each backscatter measurement; thus, the record gives both the scattered return and the output energy for each shot.

The receiver sensitivity was measured by using a standard lamp, which was calibrated by the National Bureau of Standards and was found to be 0.94 volts/μW. In order to perform this measurement, it was necessary to know the solid angle subtended by the receiver and its spectral bandwidth. With a measured half-angle field of view of 3 mrad, it was determined that the solid angle was 28 μsr. The spectral bandwidth of the system was limited by the narrow-band interference filter. An analysis of the interference filter determined that the energy received from the standard lamp was predominately within the 0.001175 μm band pass of the filter.

The alinement of the system was performed by adjusting the direction of the laser beam until a maximum return was obtained from atmospheric scattering.

Analysis of Data

The data were analyzed and compared with results from the theoretical analysis. The airplane was flown at predetermined altitudes and the laser was fired at 1 pulse/sec. Figure 7 is a typical trace obtained. This probing was taken with the airplane flying at an altitude of 0.31 km over Williamsburg, Virginia (lat. 37°17' N, long. 76°45' W). Labeled on the trace is the peak of the integrated output of the photodiode monitor, crossover of the transmitter beam and the field of view of the detector, and the normal R^{-2} falloff of the atmospheric return.

At each altitude, at least five probings were made. The output energy and the signal return at $\frac{1}{2}$-μsec intervals for each probing were later read and recorded. These data were then analyzed in the following manner: Equation (3) can be written as

$$P_r = \frac{cE_T A_r}{2R^2} f_t(h) e^{-2\beta_t(h)R} \tag{5}$$

Since for this system the range R is always very small, $e^{-2\beta_t(h)R} \approx 1$; thus,

$$P_r \approx \frac{cE_T A_r}{2R^2} f_t(h) \tag{6}$$

Now, the signal voltage at the oscilloscope can be given as

$$V\!\left(t_E\right) = P_r \times s_r \times 10^6 \text{ volts} \tag{7}$$

where

$$R = \frac{3.0}{2} t_E \times 10^2 \text{ m} \tag{8}$$

By combining equations (6), (7), and (8)

$$V\!\left(t_E\right) = \frac{\frac{2}{9} cE_T A_r s_r}{t_E^2} f_t(h) \times 10^2 \text{ volts} \tag{9}$$

The general form of the $V\!\left(t_E\right)$ distributions can be written

$$V\!\left(t_E\right) = \frac{\kappa}{t_E^2} \tag{10}$$

Combining equations (9) and (10) and solving for $f_t(h)$ yields

$$f_t(h) = \frac{9}{2} \frac{\kappa}{cE_T A_r s_r} \times 10^{-2} \text{ sr}^{-1}\text{m}^{-1} \tag{11a}$$

With $A_r = 9.48 \times 10^{-3}$ m,

$$f_t(h) = \frac{1.58\kappa}{E_T s_r} \times 10^{-8} \text{ sr}^{-1}\text{m}^{-1} \tag{11b}$$

9

Thus, to arrive at the total experimental scattering function, it is necessary to measure the curve constant κ, the total energy E_T, and the receiver sensitivity s_r.

Error Analysis

Two types of error are considered to influence the results of the experimental data. The first is an absolute error associated with the calibration equipment and technique, and the second is a random error arising from system fluctuations and data reduction. The absolute error is estimated to be ±25 percent based on ±10 percent error in the transmitter calibration due to calorimeter uncertainty, and ±15 percent in the receiver calibration. The random errors considered are estimated as follows:

	Root-mean-square error, percent
Photomultiplier electron emission (shot noise)	±5
Output monitor	±3
Frequency stability of 400 Hz power supply	±2
Reading error	±3

These errors are considered to be independent of each other and, therefore, combine as the square root of the sum of the squares to give a 1-σ value of ±6.9 percent. With a minimum of 5 probings used to compute the average scattering function for each altitude, the overall random root-mean-square error reduces to $\sigma/\sqrt{5}$ (3.06 percent). The overall 3-σ error then is 9.18 percent. Therefore, the values of scattering function presented in this report are considered to be absolute within ±34 percent. This percentage applies only to data obtained in flights 28, 29, and 31 for which the output power was monitored in flight.

Results

Figure 8 presents a comparison between the experimental results obtained on March 9, 1967, over Williamsburg, Virginia (lat. 37°17' N, long. 76°45' W), and the calculated theoretical model. Each datum point represents the average scattering function for that altitude taken from five consecutive laser probings. For each probing the total transmitted energy was measured, and the curve constant κ was obtained by computing the best fit t^{-2} curve to the signal-versus-time data. (See fig. 7.) The experimental data are seen to be in very good agreement with the theoretical predictions.

Figure 9 presents a composite of additional data taken from March 1966 to April 1967 near Williamsburg, Virginia and over the local coastal region of the Atlantic Ocean. These data tend to support the theoretical model; however, there are two important points to be made. The first is that a measure of the output energy for each pulse is almost

essential for probings of this nature. For the data shown for all flights before flight number 28, the output energy was taken to be the average of measurements made on the ground before and after each flight. From flight 28 on, the energy was measured for each pulse while in flight. The results show that the scattering functions measured in flights 28 through 31 are in closer agreement with the theoretical model than results from earlier flights.

The second point is in regard to defining scattering of a clear atmosphere. Since the only basis for classifying clear air was from pilot's and observer's notes recorded in the flight log, there is obviously room for questioning the term "clear air." The three data points shown for flight 31 at an altitude of about 9 km were taken in a very light haze layer. While there is considerable variation of scattering function between the samples, all three are considerably greater than the data taken in the air judged to be "clear."

Although the system was sufficiently sensitive to provide a measure of the atmospheric scattering function, it did not have sufficient performance capability to probe small horizontal scattering changes that might be associated with such phenomena as wind shear layers, temperature gradients, and possibly clear-air turbulence.

APPLICATION OF THE MODEL TO LASER SYSTEM DESIGN

Introduction

In the preceding sections a model was developed to describe the backscatter of ruby-laser light in a clear atmosphere. In the following section the model has been used to generate a series of parametric curves to aid investigators in the evaluation of detection capabilities for existing systems and to aid in the design of a system based on some predetermined detection criteria. The signal detectability of a system is discussed for three hypothetic atmospheric conditions:

Condition I is total signal detectability; the molecular and aerosol densities are horizontally uniform and adhere to the model shown for the total scattering function.

Condition II is molecular signal detectability; the molecular and aerosol densities conform to the model out to a horizontal range R; at and beyond R, an increase or decrease in the molecular density exists.

Condition III is aerosol signal detectability; the molecular and aerosol densities conform to the model out to a horizontal range R; at and beyond R, an increase or decrease in aerosol density exists.

For all conditions the relationship between signal detectability, the altitude of the test vehicle, and the horizontal range R is given.

Several examples are provided to illustrate the use of the curves. Also presented are analyses of detection capabilities for the system used in verification of the model and a proposed improved system which is within the present state of the art.

Derivation of Parametric Curves

Condition I: total signal detectability.- By using equation (3) the total number of photoelectrons produced at the photocathode of the receiver in counting time t_c is

$$N_{e,t} = \frac{\zeta c Q E_T}{4R^2} f_t(h) e^{-2\beta_t(h)R} \tag{12}$$

where

$$Q = 2A_r t_c \gamma \eta = \frac{A_r \gamma \eta}{\Delta B}$$

The S/N value for total signal detection is

$$\frac{S}{N} = \frac{N_{e,t}}{\sqrt{N_{e,t} + N_{e,D} + N_{e,B}}} \tag{13}$$

where $N_{e,D}$ is the number of thermal electrons (dark current) and $N_{e,B}$ is the number of electrons due to sky brightness. It is assumed that $N_{e,t} \gg N_{e,D} + N_{e,B}$; this assumption is discussed in appendix F. Equation (13) then reduces to

$$\frac{S}{N} = \sqrt{N_{e,t}} \tag{14}$$

Substitution of equation (12) into (14) yields

$$\sqrt{\frac{QE_T}{R^2}} = \frac{6.17\left(\frac{S}{N}\right)}{\sqrt{f_t(h)}} e^{\beta_t(h)R} \times 10^{-1} \tag{15}$$

Neglecting, for the moment, attenuation, both sides of equation (15) can be set equal to a parametric variable K:

$$K = \frac{6.17\left(\frac{S}{N}\right)}{\sqrt{f_t(h)}} \times 10^{-14} \tag{16}$$

12

and

$$K = \sqrt{\frac{QE_T}{R^2}} \qquad (17)$$

By using equation (16), K is plotted as a function of altitude for $S/N = 1$ and $\sqrt{10}$ in figure 10. Figure 11 gives the relationship (eq. (17)) between QE_T and R for various constant values of K. By using the curves in figures 10 and 11, it is possible to (A) determine an existing system's detection capability, and (B) select system parameters to meet predetermined detection criteria. In determining a system's detection capabilities, a maximum range of the system is determined for a given QE_T. This range R must be corrected for attenuation. Referring to equation (12), the relationship between predicted range R and range corrected for attenuation R_C is

$$R = R_C e^{\beta_t(h)R_C}$$

This relationship is plotted for constant values of $\beta_t(h)$ in figure 12. To determine R_C the value of $\beta_t(h)$ from figure 13 corresponding to the value of h used in determining R is used. The intersection of this $\beta_t(h)$ curve in figure 12 with the value of R then determines R_C.

In selecting the system parameters to meet predetermined detection criteria, the quality factor QE_T of a laser system is determined for a given range R. This factor must also be corrected for attenuation effects. By referring to equation (12), the correction to QE_T is

$$\left(QE_T\right)_C = QE_T e^{2\beta_t(h)R}$$

The correction factor $e^{2\beta_t(h)R}$ is plotted for constant values of $\beta_t(h)$ as a function of range R in figure 14. $\beta_t(h)$ is determined from figure 13 and the correction factor from figure 14 is applied to the predicted quality factor QE_T as above to obtain $\left(QE_T\right)_C$.

A procedure for making both of these determinations with examples is as follows:

(A) Determination of an existing system's detection capability
    (1) Using known or measured parameters of the system, calculate QE_T.
    (2) Select an altitude and minimum S/N value desired $\left(S/N = 1 \text{ or } \sqrt{10}\right)$, and refer to figure 10 to determine the corresponding value of K.
    (3) Refer to figure 11 and determine the value of R at which the constant K curve found in step (2) crosses the known value of QE_T. This value of R indicates the maximum detection range.

(4) Correct for attenuation as outlined above.

Example

(1) Given: $QE_T = 6.61 \times 10^{-15}$ J-sec-m^2 in the present system.

(2) Select $h = 0.31$ km and $S/N = \sqrt{10}$.

(3) By referring to figure 10, $K = 1.6 \times 10^{-10}$ is obtained. By using this value in figure 11(c) (as illustrated), a maximum range of 5×10^2 m is obtained.

(4) $R_C = 4.8 \times 10^2$ m.

This example illustrates the low sensitivity of the present airborne laser system. The altitude in this example was chosen to match the altitude at which the sample oscilloscope trace, figure 7, was taken. As can be seen in figure 7 at a range of 4.8×10^2 m, the S/N value is approximately $\sqrt{10}$.

(B) Selection of system parameters to meet predetermined detection criteria

(1) Predetermined detection criteria specify altitude h, range R, and S/N value.

(2) From figure 10, determine the value of K which corresponds to the predetermined values of h and S/N.

(3) From figure 11, determine the value of QE_T at which the line corresponding to value of K found in step (2) crosses the predetermined value of R.

(4) Correct for attenuation as outlined previously.

Example

(1) Given: $h = 10$ km, $R = 10^4$ m, $S/N = \sqrt{10}$.

(2) From figure 10, $K = 4.8 \times 10^{-10}$.

(3) From figure 11, it is determined that the constant $K = 4.8 \times 10^{-10}$ curve crosses $R = 10^4$ m at a value of $QE_T = 2.3 \times 10^{-11}$ J-sec-m^2.

(4) $\left(QE_T\right)_C = QE_T(1.08)$ J-sec-m^2
$= 2.5 \times 10^{-11}$ J-sec-m^2

Condition II: molecular signal detectability.- For this condition, it is assumed that there exists a clear atmosphere in front of the test vehicle to a range R, at which there is an instantaneous change in the molecular density with no change in the aerosol density. As in equation (12), the number of photoelectrons due solely to molecules can be written as

$$N_{e,R} = \frac{\zeta c Q E_T}{4R^2} f_R(h) e^{-2\beta_t(h)R}$$

With a percent change in molecular density m, the signal-to-noise ratio is

$$\frac{S_m}{N} = \frac{mN_{e,R} \times 10^{-2}}{\sqrt{N_{e,t}}}$$

This then gives

$$\sqrt{\frac{QE_T}{R^2}} = K = \frac{6.17 \frac{S_m}{N} \sqrt{f_t(h)}}{mf_R(h)} \times 10^{-12}$$

neglecting attenuation. A family of curves for constant values relating m with altitude is shown in figure 15 for both $S_m/N = 1$ and $\sqrt{10}$. The procedure for utilizing these curves with an example is given below:

(A) Determination of an existing system's detection capability
The procedure is the same as that given for (A) in condition I, except for step (2). In step (2), select also a percent change in molecular density m and then refer to figure 15 for the corresponding value of K.

(B) Selection of system parameters to meet predetermined detection criteria
The procedure is the same as that given for (B) in condition I except in step (1) a percent change in molecular density m is also predetermined and in step (2) figure 15 is referred to for the corresponding value of K.
Example
(1) Given: h = 16 km, $R = 10^4$ m, $S_m/N = \sqrt{10}$, m = 1 percent.
(2) From figure 15, $K = 9 \times 10^{-8}$.
(3) From figure 11(a), it is determined that the constant $K = 9 \times 10^{-8}$ curve crosses $R = 10^4$ m for a $QE_T = 8.0 \times 10^{-7}$ J-sec-m^2.
(4) With h = 10 km from figure 13 $\beta_t(h) = 2.0 \times 10^{-6}$ m^{-1}. By referring to figure 14, the correction factor for $R = 10^4$ m is 1.08; therefore,

$$\left(QE_T\right)_C = 8.0 \times 10^{-7}(1.08) \text{ J-sec-m}^2 = 8.64 \times 10^{-7} \text{ J-sec-m}^2$$

Condition III: aerosol signal detectability.- This procedure is analogous to that of condition II. It is found that with attenuation neglected

$$\sqrt{\frac{QE_T}{R^2}} = K = \frac{6.17 \frac{S_a}{N} \sqrt{f_t(h)}}{af_M(h)} \times 10^{-12}$$

A family of curves for constant values of K relating a with altitude is shown in figure 16 for both $S_a/N = 1$ and $\sqrt{10}$. The procedures for utilizing these curves are given below:

(A) Determination of an existing system's detection capability

The procedure is the same as given for (A) in condition I except a value for percent change in aerosol density a instead of m is selected and the value of K is obtained from figure 16.

(B) Selection of system parameters to meet predetermined detection criteria

The procedure is the same as given for (B) in condition II except a percent change in aerosol density a instead of m is predetermined and figure 16 is referred to for the corresponding value of K.

It should be noted that although a distinction is made in conditions II and III between the molecular and aerosol density changes, the laser system measures only total scattering and cannot distinguish between the two.

Use has been made of these curves to predict the maximum range R_C as a function of altitude for two systems: the present system $\left(QE_T = 6.61 \times 10^{-15}\right)$ and an improved system $\left(QE_T = 3.75 \times 10^{-10}\right)$. Table III summarizes the characteristics of these two systems. Shown in figure 17 is the predicted maximum range R_C capability for signal detectability of a clear atmosphere for a S/N value of $\sqrt{10}$. In figure 18 the maximum range R_C as a function of altitude for the improved system is plotted for the detection of a 1-percent change in molecular density with a S_m/N ratio value of 1; the present system could not make this detection for a range greater than 10^2 meters at any altitude.

Figure 19 gives the maximum range R_C for the improved system as a function of altitude for the detection of a 10-percent change in aerosol density with S_a/N equal to 1. These design curves should be very valuable to investigators either presently involved in an airborne laser program or contemplating the initiation of such a program. They provide a means of quickly determining either the capabilities of their present system or system parameters necessary to fulfill the objectives of their programs.

CONCLUDING REMARKS

A theoretical model of ruby-laser radiation backscatter with a wavelength of 0.6943 μm in the lower atmosphere has been developed. This model includes not only molecular scattering based on Rayleigh theory but also atmospheric aerosol scattering based on Mie theory.

Based on this model and the measurements made, it appears that molecular scattering predominates in the altitude range of 4 to 14 km.

This model has been verified up to an altitude of 11 km by using a laser system installed in a jet airplane. The system was found to be satisfactory for measuring the average scattering function and results were in good agreement with the model.

The airborne system did not, however, have sufficient performance capability to probe the small horizontal scattering changes that might be associated with such phenomena as wind shear layers, temperature gradients, and possibly clear-air turbulence. A set of design parametric curves for an airborne laser probing system has been derived based on the theoretical model. These design curves should be very valuable to investigators either presently involved in an airborne laser program or contemplating the initiation of such a program. They provide a means of quickly determining either the capabilities of their present system or system parameters necessary to fulfill the objectives of their programs.

Langley Research Center,
        National Aeronautics and Space Administration,
                Langley Station, Hampton, Va., September 12, 1969.

APPENDIX A

DERIVATION OF GENERAL SCATTERING EQUATION

The equation below gives a fundamental relationship between the power transmitted and the power received:

$$\frac{P_r}{P_T} = \frac{\sigma_R(\theta,\lambda)N_R(h) + \sigma_M(\theta,\lambda)N_M(h)}{A_T(R)R^2} A_r e^{-2\beta_t(h)R} \tag{A1}$$

where $R^2 \gg A_r$ and $A_T(R)$. The total number of Rayleigh and Mie scattering centers can be related to Rayleigh and Mie number densities, respectively, by

$$N_R(h) = n_R(h)v \tag{A2}$$

$$N_M(h) = n_M(h)v \tag{A3}$$

The scattering volume in terms of the laser pulse width is

$$v = c\tau A_T(R) \tag{A4}$$

The average power transmitted per pulse can be related to the total transmitted energy by

$$P_T = \frac{E_T}{\tau} \tag{A5}$$

Substitution of equations (A2), (A3), (A4), and (A5) into equation (A1) yields

$$P_r = \frac{cE_T A_r}{2R^2}\left[\sigma_R(\theta,\lambda)n_R(h) + \sigma_M(\theta,\lambda)n_M(h)\right]e^{-2\beta_t(h)R}$$

where the factor of 2 in the denominator is due to the conversion of the time variable to oscilloscope time.

APPENDIX B

DERIVATION OF RAYLEIGH SCATTERING FUNCTION

Although the incident laser radiation is polarized, unpolarized scattering theory for $\theta = 0^{\circ}$ or 180° predicts correct results; therefore, it will be assumed for purposes of calculation that the incident light is unpolarized. Thus, the cross section for scattering due to molecules in the notation of the present report can be shown in reference 13 to be

$$\sigma_R(\theta,\lambda) = \frac{\left(1 + \cos^2\theta\right)k^4|\overline{\alpha}|^2 F}{2} \times 10^{24} \quad m^2 sr^{-1} \tag{B1}$$

The equation for the anisotropy factor from reference 13 is

$$F = \frac{3(2 + D)}{6 - 7D}$$

where D has been found to be 0.03 (ref. 14); thus, $F = 1.05$. With $\theta = 180^{\circ}$, $\lambda = 0.6943 \ \mu m$, and $\overline{\alpha} \approx 1.73 \times 10^{-30}$ n (ref. 15),

$$\sigma_R(180^{\circ}, 0.6943 \ \mu m) = 2.10 \times 10^{-32} \quad m^2 sr^{-1} \tag{B2}$$

Substituting equation (B2) into equation (2), the scattering function due to molecules is obtained as a function of molecular number density:

$$f_R(180^{\circ}, 0.6943 \ \mu m, h) = 2.10 \times 10^{-32} \ n_R(h) \quad sr^{-1}m^{-1} \tag{B3}$$

APPENDIX C

DERIVATION OF MIE SCATTERING FUNCTION

Scattering due to aerosols is more difficult to analyze than that due to molecules. Aerosols consist of a variety of airborne particles and include water or fog droplets, dust, and combustion products. The difficulty arises because the size of these particles generally is on the order of the wavelength of the incident light, and resonances may occur.

Again, by using the unpolarized incident-light theory, the cross section for scattering by aerosols is shown in reference 13 to be

$$\sigma_M(\theta,\lambda) = \frac{i_1(\theta,\lambda,\iota,p) + i_2(\theta,\lambda,\iota,p)}{2k^2} \times 10^{-12} \text{ m}^2\text{sr}^{-1} \tag{C1}$$

where i_1 and i_2 are the Mie scattering amplitudes and are a function of the angle θ, the wavelength of the incident light λ, the relative index of refraction of the particles ι, and the shape of the aerosols p. The shape of the aerosols is assumed to be spherical. This assumption is reasonable since many of the particles are liquid, and these tend to form spheroids. It is also a necessary assumption since the scattering amplitudes have been calculated for spheres, but little work has been done for other shapes. Tabulation of Mie scattering amplitudes calculated before 1957 is given in reference 13. More recent tabulations for spherical particles are reported in reference 16. The average index of refraction will be assumed to be 1.50. (See, refs. 13 and 17.) This assumption is based on the discovery of dissolved salts in the liquid aerosols. (See ref. 18.) Based on these assumptions and with $\theta = 180^O$ and $\lambda = 0.6943 \mu m$ the cross section for scattering due to aerosols is

$$\sigma_M(180^O, 0.6943 \ \mu m) = \frac{i_1(180^O, 0.6943 \ \mu m, 1.50, r) + i_2(180^O, 0.6943 \ \mu m, 1.50, r)}{2k^2} \times 10^{-12} \text{ m}^2\text{sr}^{-1} \tag{C2}$$

In order to use equation (C2) in equation (2) of the text, it is necessary to know the size distributions of the atmospheric aerosols. Investigations of the size distribution of atmospheric aerosols have been performed by Junge (ref. 19) and others (see, for example, refs. 20 and 21). Junge's measurements were made over the European Continent but agree well with data taken near Baltimore, Maryland (ref. 20). The distribution from $r \approx 20 \ \mu m$ to $r \approx 0.1 \ \mu m$ is given as

$$dn_M(r,h) = C(h)r^{-3} \ d \log r \tag{C3a}$$

then

$$d \log r = 0.434 r^{-1} \, dr$$

and

$$dn_M(r,h) = C'(h) r^{-4} \, dr \qquad \text{(C3b)}$$

This distribution has been reported by Junge (ref. 22) to be invariant with altitude in the lower atmosphere.

Substituting equations (C2) and (C3b) into equation (2) and integrating yields

$$f_M(180^\circ, 0.6943 \, \mu m, h) = C'(h) \int_{r_1}^{r_2} \frac{i_1(1.50, r) + i_2(1.50, r)}{2k^2} r^{-4} \, dr \times 10^{-6} \, sr^{-1} m^{-1}$$

$$\text{(C4)}$$

By changing the variable from the radius r to a nondimensional size parameter g, where $g = 2\pi r/\lambda$ and substituting $k = 2\pi/\lambda$, it can be shown from equation (C4) that

$$f_M(180^\circ, 0.6943 \, \mu m, h) = C'(h) \frac{\pi}{\lambda} \int_{g_1}^{g_2} \frac{i_1(g, 1.50) + i_2(g, 1.50)}{g^4} \, dg \times 10^{-6} \, sr^{-1} m^{-1}$$

$$= C'(h) \frac{\pi}{\lambda} I \times 10^{-6} \qquad \text{(C5)}$$

where

$$I = \int_{g_1}^{g_2} \frac{i_1(g, 1.50) + i_2(g, 1.50)}{g^4} \, dg$$

Integrals similar to that in equation (C5) have been evaluated numerically in reference 17 for a number of wavelengths. These results over a size range of $r_1 = 0.04 \, \mu m$ to $r_2 = 10 \, \mu m$ are given to the third significant place as

$$I = 0.442 \qquad \text{(C6)}$$

The constant C' in equation (C5) can be evaluated in terms of the total aerosol number density by integrating equation (C3b) over the size limits consistent with data obtained near Chesapeake Bay (ref. 23):

$$n_M(h) = \int_{0.1}^{20} dn_M(r,h) = C'(h)\int_{0.1}^{20} r^{-4}\ dr \tag{C7a}$$

or

$$C'(h) = 3n_M(h) \times 10^{-3} \tag{C7b}$$

By substituting this value for $C'(h)$ and the value of the integral from equation (C6) into equation (C5), the scattering function due to aerosols becomes

$$f_M(180^O,\ 0.6943\ \mu m,\ h) = 6.0 \times 10^{-9}\ n_M(h)\ sr^{-1}m^{-1} \tag{C8}$$

APPENDIX D

AEROSOL NUMBER DENSITY AS A FUNCTION OF ALTITUDE

In 1961, a sea-level measurement near Chesapeake Bay of the total aerosol number density was made. (See ref. 23.) This measurement was performed by fitting light-attenuation data to theoretical predictions. The theory was based on the same assumptions as presented in appendix C, that is, spherical aerosols with index of refraction of 1.50 and Junge's size distribution from $r_1 = 0.1$ μm to $r_2 = 20$ μm. The results taken on a clear day with a visibility of 25 km yielded a total aerosol number density of approximately 215 particles/cm^3.

Total number density as a function of altitude has been measured. All measurements made before 1954 are summarized in reference 24. It was found that the density decreased exponentially with altitude up to 5 km. The scale height of the decrease in aerosols was determined to be 1.2 km. Aerosol densities up to an altitude of 26 km were measured in 1965. (See ref. 25.) The aerosol number density at kilometer intervals is shown in table I. The aerosol number density from reference 25 was corrected since aerosols with radii greater than 0.125 μm were measured; and to be consistent with the densities from reference 24, it was necessary to correct these values to a lower limit of 0.10 μm by assuming the Junge distribution given in equations (C3a) and (C3b). Because the value for the number density at 5 km differed in the two investigations (refs. 24 and 25), the average value at this altitude was used.

Another tabulation of aerosol number density as a function of altitude is presented in reference 26. The aerosol data which were used herein were obtained from reference 27 for an altitude range of 10 to 25 km. These data are an order of magnitude below those used in the present report from reference 25. The justification for using the data of reference 25 is that it predicts an increase in scattering greater than Rayleigh prediction above an altitude of 16 km; this result has been observed by a number of investigators. (See refs. 6, 28, and 29.) Data plotted in figure 20 from reference 29 is typical of the increased scattering in the 16- to 26-km altitude region reported by the other two investigators (refs. 6 and 28).

APPENDIX E

DETERMINATION OF ATMOSPHERIC EXTINCTION COEFFICIENT

The total atmospheric extinction coefficient can be written as

$$\beta_t(h) = \beta_R(h) + \beta_M(h) + \beta_O(h) \tag{E1}$$

$\beta_R(h)$ can be calculated by integrating the Rayleigh scattering function over all space as

$$\beta_R(h) = \int_0^{2\pi} d\phi \int_0^{\pi} d\theta \sigma_R(\theta,\lambda)\sin\theta n_R(h) \tag{E2}$$

or by combining equations (B1) and (E2)

$$\beta_R(h) = \int_0^{2\pi} d\phi \int_0^{\pi} d\theta \frac{(1 + \cos^2\theta)k^4|\bar{\alpha}|^2}{2} Fn_R(h) \times 10^{24} \tag{E3}$$

which, for $\lambda = 0.6943$ μm, gives

$$\beta_R(h) = 17.6n_R(h) \times 10^{-32} \text{ m}^{-1} \tag{E4}$$

Now, at sea level $\beta_O(0) \approx 0$ and $\beta_t(0) \approx 0.135 \times 10^{-3}$ m^{-1} (from ref. 23 for a visibility of 25 km); therefore, from equation (E1)

$$\beta_M(0) = 0.131 \times 10^{-3} \text{ m}^{-1} \tag{E5}$$

since

$$\beta_R(0) = 4.24 \times 10^{-6} \text{ m}^{-1} \tag{E6}$$

An effective extinction cross section for aerosols can be calculated from

$$\beta_M(0) = n_M(0)\sigma_M \tag{E7}$$

where σ_M is the Mie extinction cross section. Based on data from table I, where

$$n_M(0) = 215 \text{ cm}^{-3}$$

$$\sigma_M = 6.09 \times 10^{-7} \ cm^3m^{-1}$$

The extinction cross section as a function of altitude then is

$$\beta_M(h) = 6.09 n_M(h) \times 10^{-7} \ m^{-1} \tag{E8}$$

and the total extinction coefficient obtained by combining equations (E1), (E4), and (E8) is

$$\beta_t(h) = 17.6 n_R(h) \times 10^{-32} + 6.09 n_M(h) \times 10^{-7} + \beta_O(h) \ m^{-1}$$

where $n_R(h)$ is obtained from reference 12, $n_M(h)$ is obtained from table I, and $\beta_O(h)$ is obtained from reference 25.

APPENDIX F

ON THE ASSUMPTION $N_{e,t} \gg N_{e,D} + N_{e,B}$

The number of electrons at the photocathode due to dark current in a counting time is

$$N_{e,D} = \frac{J_{A,D}}{G} t_c (6.25 \times 10^{18}) \text{ electrons}$$

or

$$N_{e,D} = \frac{J_{A,D}}{2BG} (6.25 \times 10^{18}) \text{ electrons}$$

The number of photoelectrons produced at the photocathode of the receiver by the daylight sky brightness is

$$N_{e,B} = b\Omega_r \Delta\nu A_r t_c \eta\gamma\zeta \times 10.76 \text{ photoelectrons}$$

or

$$N_{e,B} = b\Omega_r \Delta\nu Q\zeta \times 5.38 \text{ photoelectrons}$$

where b is the sky brightness in $W\text{-ft}^{-2}\text{-sr}^{-1}\text{-Å}^{-1}$ and is equal to 10^{-4} in the 6000- to 7000-Å region (ref. 30). The additional parameters for the present and improved systems are shown in table III.

For the present system, $N_{e,D} + N_{e,B} = 4.95 \times 10^{-2}$ electrons and for the improved system, $N_{e,D} + N_{e,B} = 8.88 \times 10^{-2}$ electrons. For a signal-to-noise ratio of 1 or $\sqrt{10}$, $N_{e,t} = 1$ or 3.16 electrons, respectively. Therefore, for both systems and both signal-to-noise ratios the inequality $N_{e,t} \gg N_{e,D} + N_{e,B}$ is a valid assumption.

REFERENCES

1. Synge, E. H.: A Method of Investigating the Higher Atmosphere. Phil. Mag. and J. Sci., vol. 9, no. 60, May 1930, pp. 1014-1020.

2. Hulburt, E. O.: Observations of a Searchlight Beam to an Altitude of 28 Kilometers. J. Opt. Soc. Amer., vol. 27, no. 11, Nov. 1937, pp. 377-382.

3. Johnson, E. A.; Meyer, R. C.; Hopkins, R. E.; and Mock, W. H.: The Measurement of Light Scattered by the Upper Atmosphere From a Search-Light Beam. J. Opt. Soc. Amer., vol. 29, no. 12, Dec. 1939, pp. 512-517.

4. Elterman, L.: Seasonal Trends of Temperature, Density, and Pressure in the Stratosphere Obtained With the Searchlight-Probing Technique. Geophys. Res. Papers No. 29. (AFCRC TR 54-19), Air Force Cambridge Res. Center, July 1954.

5. Fiocco, G.; and Smullin, L. D.: Detection of Scattering Layers in the Upper Atmosphere (60-140 km) by Optical Radar. Nature, vol. 199, no. 4900, Sept. 28, 1963, pp. 1275-1276.

6. Clemesha, B. R.; Kent, G. S.; and Wright, R. W. H.: Laser Probing the Lower Atmosphere. Nature, vol. 209, no. 5019, Jan. 8, 1966, pp. 184-185.

7. McCormick, P. D.; Poultney, S. K.; Van Wijk, U.; Alley, C. O.; Bettinger, R. T.; and Perschy, J. A.: Backscattering From the Upper Atmosphere (75-160 km) Detected by Optical Radar. Nature, vol. 209, no. 5025, Feb. 19, 1966, pp. 798-799.

8. Bain, W. C.; and Sandford, M. C. W.: Light Scatter From a Laser Beam at Heights Above 40 km. J. Atmos. Terrest. Phys., vol. 28, no. 6/7, June/July 1966, pp. 543-552.

9. Collis, Ronald T. H.: Lidar Detection of CAT. Astronaut. Aeronaut., vol. 2, no. 12, Dec. 1964, pp. 52-54.

10. Collis, R. T. H.; and Ligda, M. G. H.: Note on Lidar Observations of Particulate Matter in the Stratosphere. J. Atmos. Sci. (Notes Corresp.), vol. 23, no. 2, Mar. 1966, pp. 255-257.

11. Franken, P. A.; Jenney, J. A.; and Rank, D. M.: Airborne Investigations of Clear Air Turbulence With Optical Radar — A Progress Report. Contract NONR 1224(51), Univ. of Michigan, Dec. 1965.

12. Anon.: U.S. Standard Atmosphere, 1962. NASA, U.S. Air Force, and U.S. Weather Bur., Dec. 1962.

13. Van de Hulst, H. C.: Light Scattering by Small Particles. John Wiley & Sons, Inc., c.1957.

14. de Vaucouleurs, G.: The Constants of Rayleigh Scattering in Gases and Liquids. Ann. Phys. (Paris), vol. 6, Mar.-Apr. 1951, pp. 213-324.

15. Böttcher, C. J. F.: Theory of Electric Polarisation, Elsevier Publ. Co., 1952.

16. Deirmendjian, D.: Tables of Mie Scattering Cross Sections and Amplitudes. U.S. Air Force Proj. RAND Rep. R-407-PR (DDC Doc. No. AD 295148), RAND Corp., Jan. 1963.

17. Bullrich, Kurt: Scattered Radiation in the Atmosphere and the Natural Aerosol. Vol. 10 of Advances in Geophysics, H. E. Landsberg and J. Van Miegham, eds., Academic Press, 1964, pp. 99-260.

18. Junge, Christian: Die Konstitution des atmosphärischen Aerosols. Ann. Meteorol., 1952.

19. Junge, Christian: The Size Distribution and Aging of Natural Aerosols as Determined From Electrical and Optical Data on the Atmosphere. J. Meteorol., vol. 12, no. 1, Feb. 1955, pp. 13-25.

20. Pasceri, Ralph E.; and Friedlander, S. K.: Measurements of the Particle Size Distribution of the Atmospheric Aerosol: II. Experimental Results and Discussion. J. Atmos. Sci., vol. 22, no. 5, Sept. 1965, pp. 577-584.

21. De Bary, E.; and Rossler, F.: Size Distributions of Atmospheric Aerosols Derived From Scattered Radiation Measurements Aloft. J. Geophys. Res., vol. 71, no. 4, Feb. 15, 1966, pp. 1011-1016.

22. Junge, Christian E.: Air Chemistry and Radioactivity. Academic Press, Inc., 1963.

23. Curcio, J. A.; Knestrick, G. L.; and Cosden, T. H.: Atmospheric Scattering in the Visible and Infrared. NRL Rep. 5567, U.S. Navy, Jan. 24, 1961. (Available from DDC as AD 250945.)

24. Penndorf, R.: The Vertical Distribution of Mie Particles in the Troposphere. AFCRC Tech. Rep. 54-5, U.S. Air Force, Mar. 1954.

25. Rosen, James M.: Correlation of Dust and Ozone in the Stratosphere. Nature, vol. 209, no. 5030, Mar. 26, 1966, p. 1342.

26. Elterman L.: Atmospheric Attenuation Model, 1964, in the Ultraviolet, Visible, and Infrared Regions for Altitudes to 50 km. Environ. Res. Papers No. 46 (AFCRL-64-740), U.S. Air Force, Sept. 1964.

27. Chagnon, Charles W.; and Junge, Christian E.: The Vertical Distribution of Sub-Micron Particles in the Statosphere. J. Meteorol., vol. 18, no. 6, Dec. 1961, pp. 746-752.

28. Grams, Gerald; and Fiocco, Giorgio: Stratospheric Aerosol Layer During 1964 and 1965. J. Geophys. Res., vol. 72, no. 14, July 15, 1967, pp. 3523-3541.

29. McCormick, Michael Patrick: Laser Backscatter Measurements of the Lower Atmosphere. Ph.D. Thesis, Coll. of William and Mary in Virginia, 1967.

30. Ross, Monte: Laser Receivers. John Wiley & Sons, Inc., c.1966.

TABLE I.- AEROSOL NUMBER DENSITY

h, km	Reference 24 $n_M(h)$, cm^{-3}	Reference 25 $n_M(h)$, cm^{-3}	Corrected $n_M(h)$, cm^{-3}	Effective $n_M(h)$, cm^{-3}
0	215			215
1	93.6			93.6
2	40.5			40.5
3	17.6			17.6
4	7.53			7.53
5	3.33	0.80	1.6	2.5
6		.65	1.3	1.3
7		.55	1.1	1.1
8		.35	.68	.7
9		.25	.49	.5
10		.35	.68	.7
11		.50	.97	1.0
12		.75	1.5	1.5
13		1.0	1.9	1.9
14		1.2	2.4	2.4
15		1.5	2.9	2.9
16		1.7	3.3	3.3
17		3.7	7.3	7.3
18		2.5	4.8	4.8
19		1.7	3.4	3.4
20		1.2	2.4	2.4
21		1.0	2.0	2.0
22		.80	1.6	1.6
23		.70	1.4	1.4
24		.65	1.3	1.3
25		.60	1.2	1.2
26		.50	.97	1.0

TABLE II.- CHARACTERISTICS OF THE TRANSMITTER AND RECEIVER SUBSYSTEMS

Transmitter subsystem:

    Laser transmitter . . . . Ruby

    Wavelength, μm 0.6943

    Peak power output, MW 10

    Total energy output, J 0.1

    Q-switching technique . . . . Saturable filter (cryptocyanine in nitrobenzene)

    Output pulse duration, nsec 20

    Beam divergence after collimating optics (total), mrad 1

    Pulse repetition rate, pulse/sec 1

    Output monitor . . . . Photodiode

Receiver subsystem:

    Receiving optics:

        Effective aperture, mm 110

        Acceptance half-angle, mrad 3

    Interference filter:

        Center wavelength, μm 0.6944375

        Optical bandwidth, μm 0.001175

        Transmission, percent 15

    Photomultiplier:

        Overall voltage, volts 1800

        Stages 16

        Quantum efficiency . . . . ≈0.003

        Photocathode response S-20

        Photocathode diameter, mm 4.83

        Additional amplifier gain 10

TABLE III.- PARAMETERS OF PRESENT AND IMPROVED SYSTEMS

Parameter	Present system	Improved system
γ	0.15	0.60
η	2.8×10^{-3}	2.5×10^{-2}
A_r, m^2	9.48×10^{-3}	0.125
B, sec^{-1}	50×10^6	5×10^6
Q, $sec\text{-}m^2$	7.97×10^{-14}	3.75×10^{-10}
E_T, joules	0.083	1
QE_T, $J\text{-}sec\text{-}m^2$	6.61×10^{-15}	3.75×10^{-10}
$J_{A,D}$, amperes	6×10^{-11}	6×10^{-11}
G	8×10^5	8×10^5
Total field of view, mrad	6	0.2
Ω_r, sr	28×10^{-6}	6.27×10^{-8}
$\Delta\nu$, Å	11.75	2.0
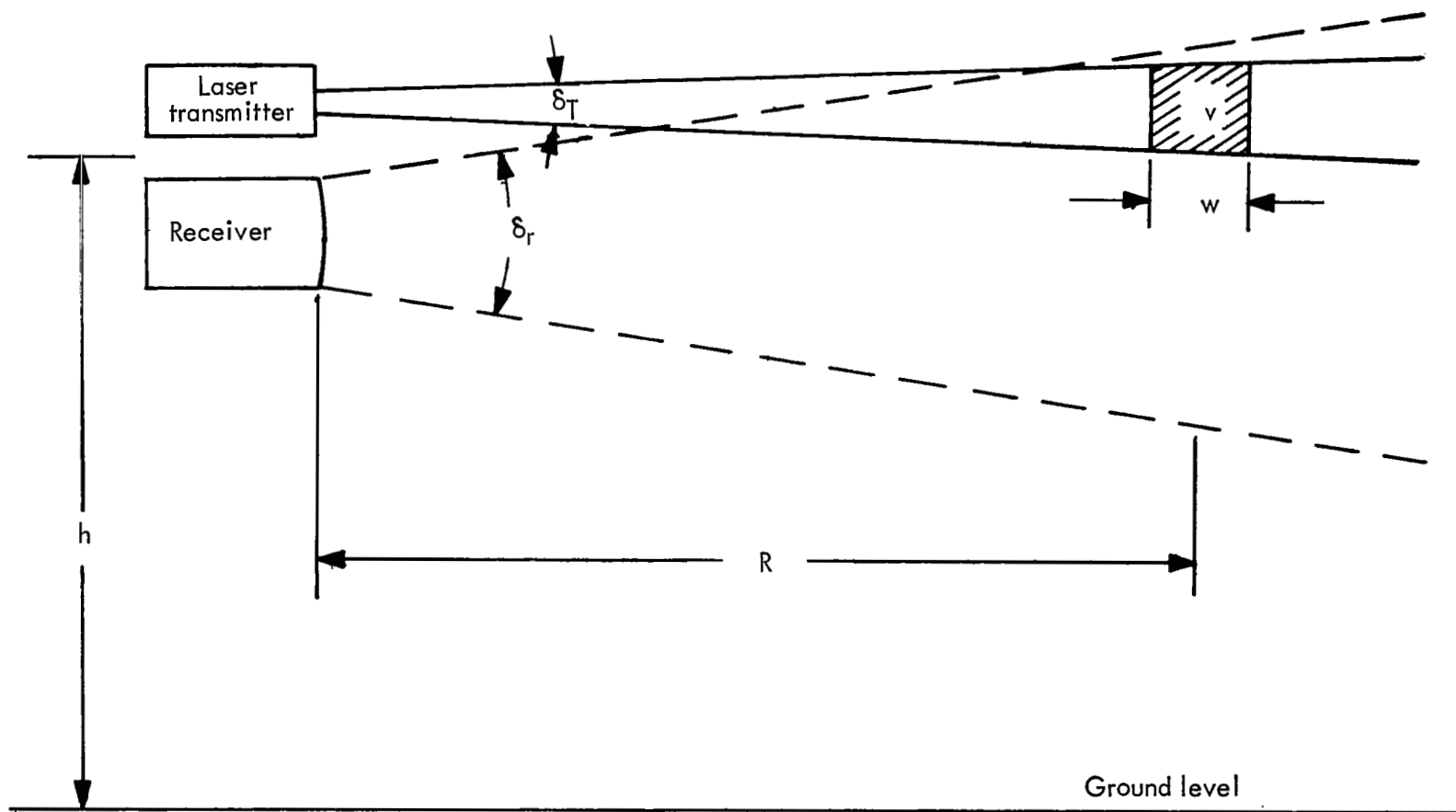
Figure 1.- Basic representation of airborne atmospheric light backscatter investigation.
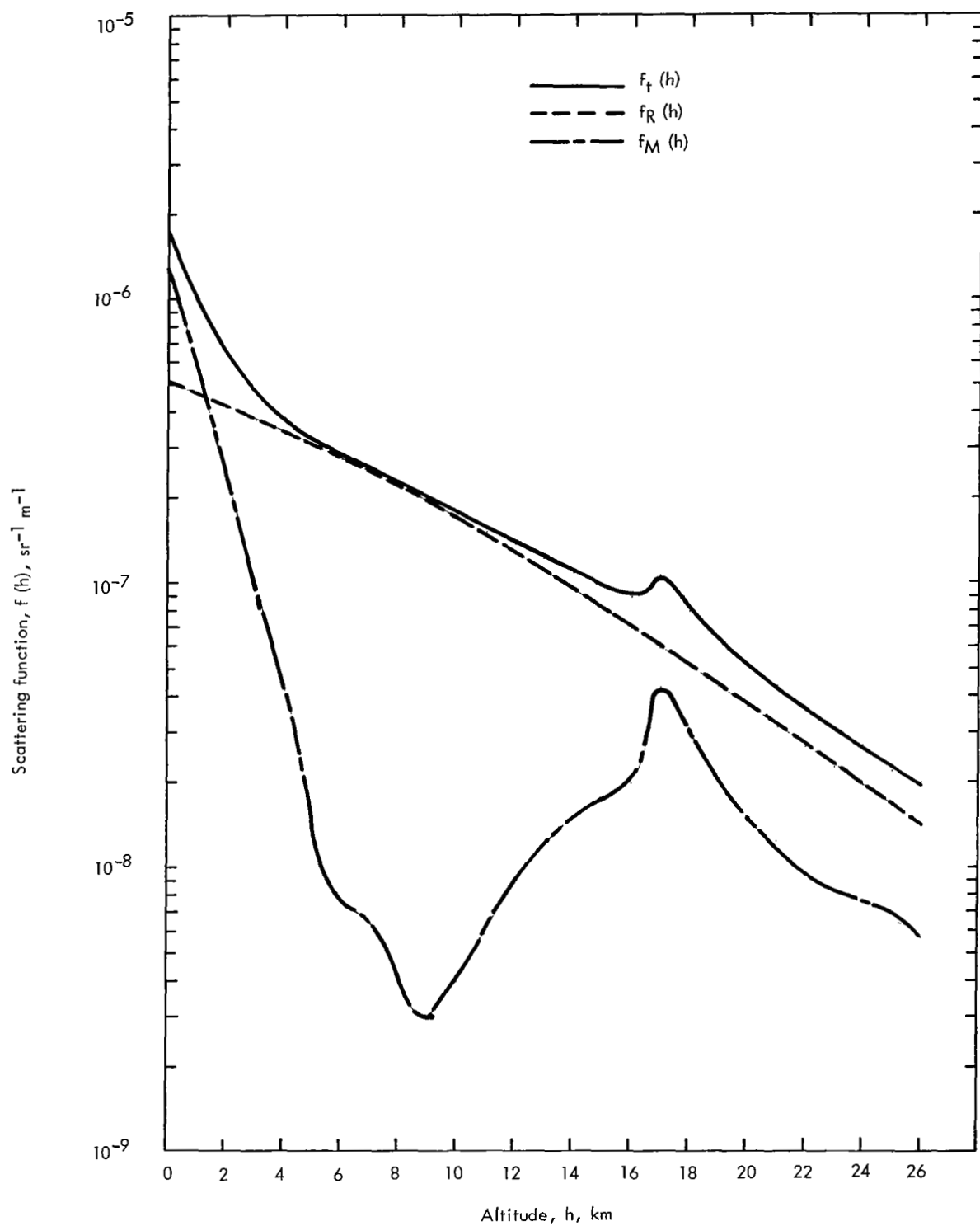
Figure 2.- Model for ruby-laser-radiation (λ = 0.6943 µm) backscatter in lower atmosphere.
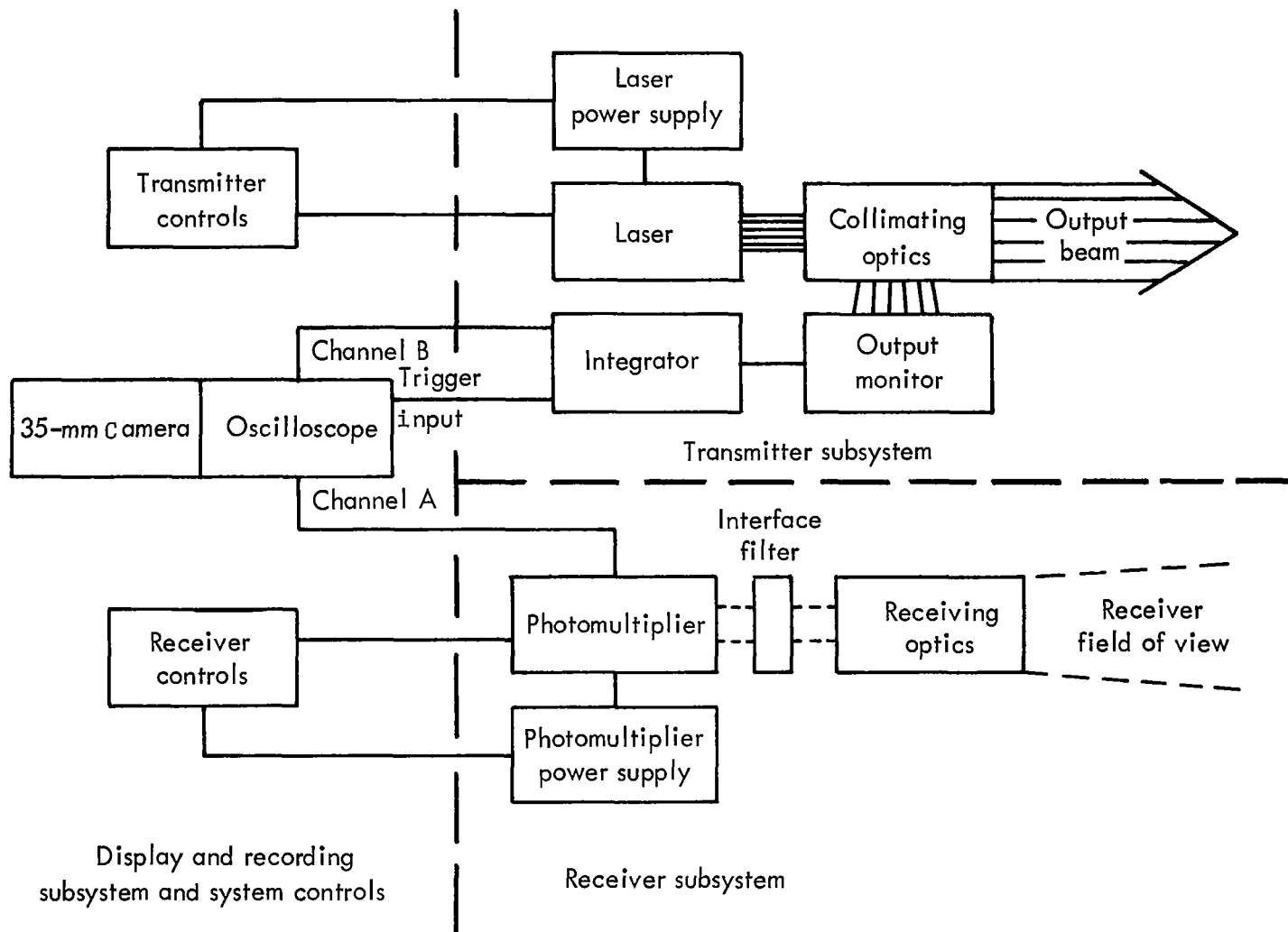
Figure 3.- Block diagram of the airborne laser system used in this investigation.
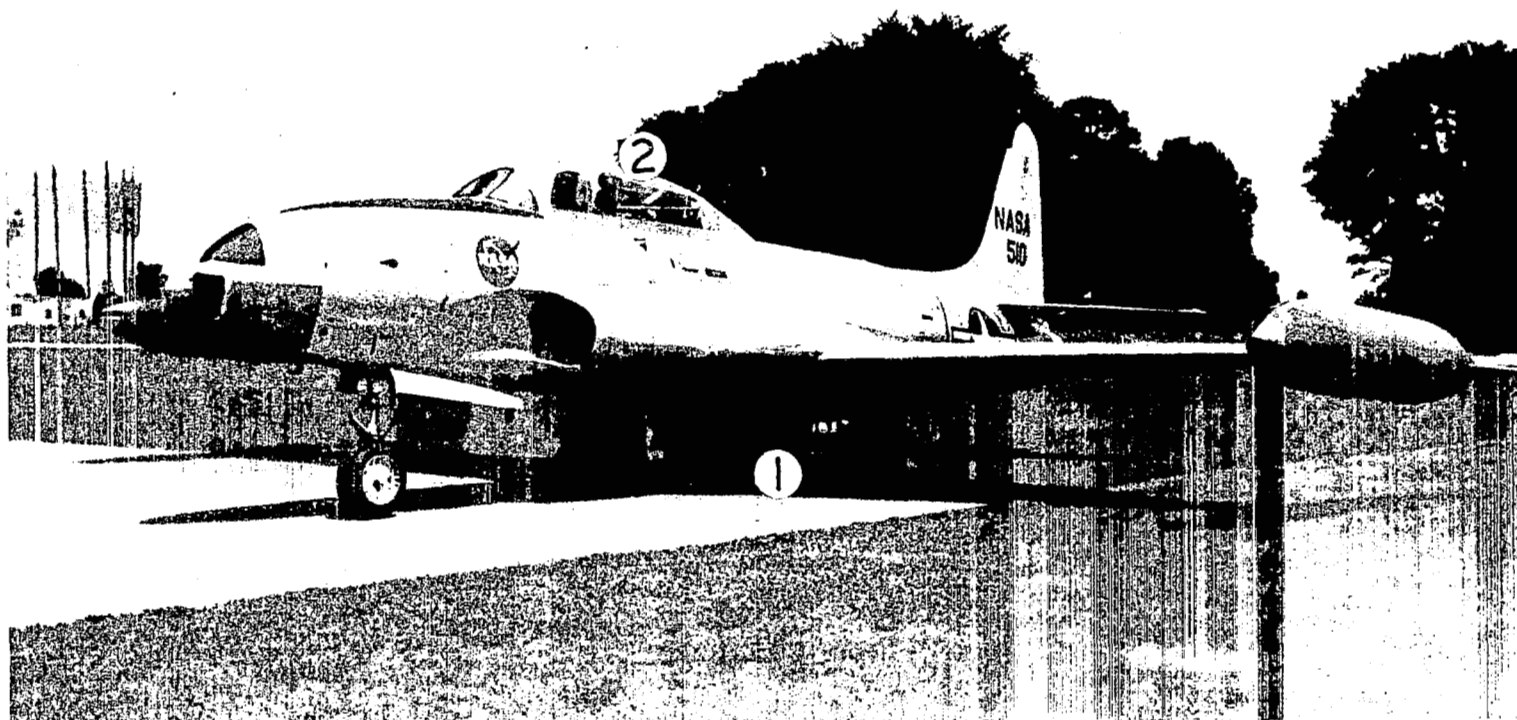
L-65-6572.1

Figure 4.- The laser system installed in a T-33 jet airplane with the location of the equipment noted as (1) transmitter and receiver subsystems and (2) display and recording subsystem and the system controls.
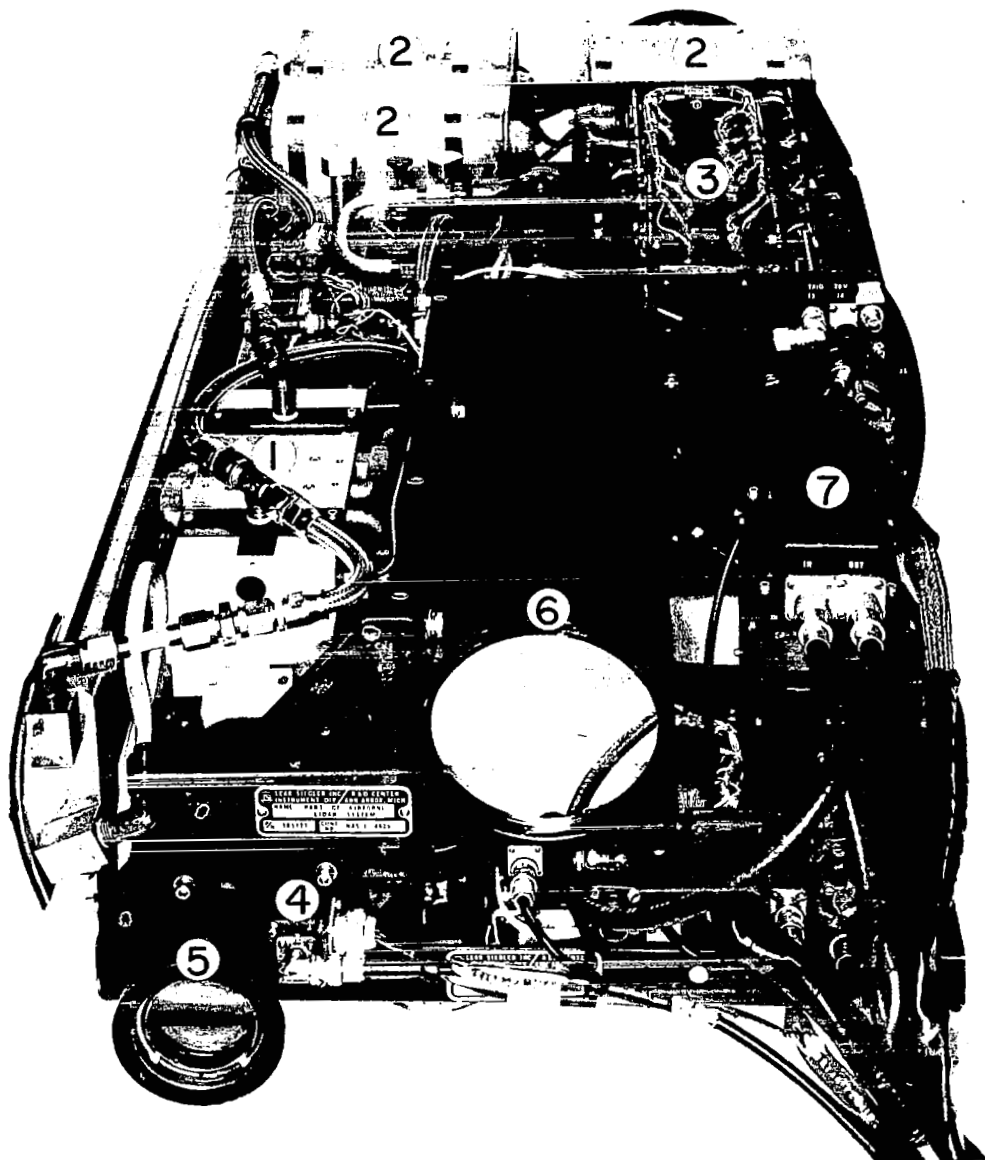
①	Laser transmitter	④	Output monitor
②	Storage capacitors	⑤	Transmitting optics
③	Laser power supply	⑥	Receiver
	⑦	Receiver power supply	

Figure 5.- Transmitter and receiver subsystems.

L-67-6365.1
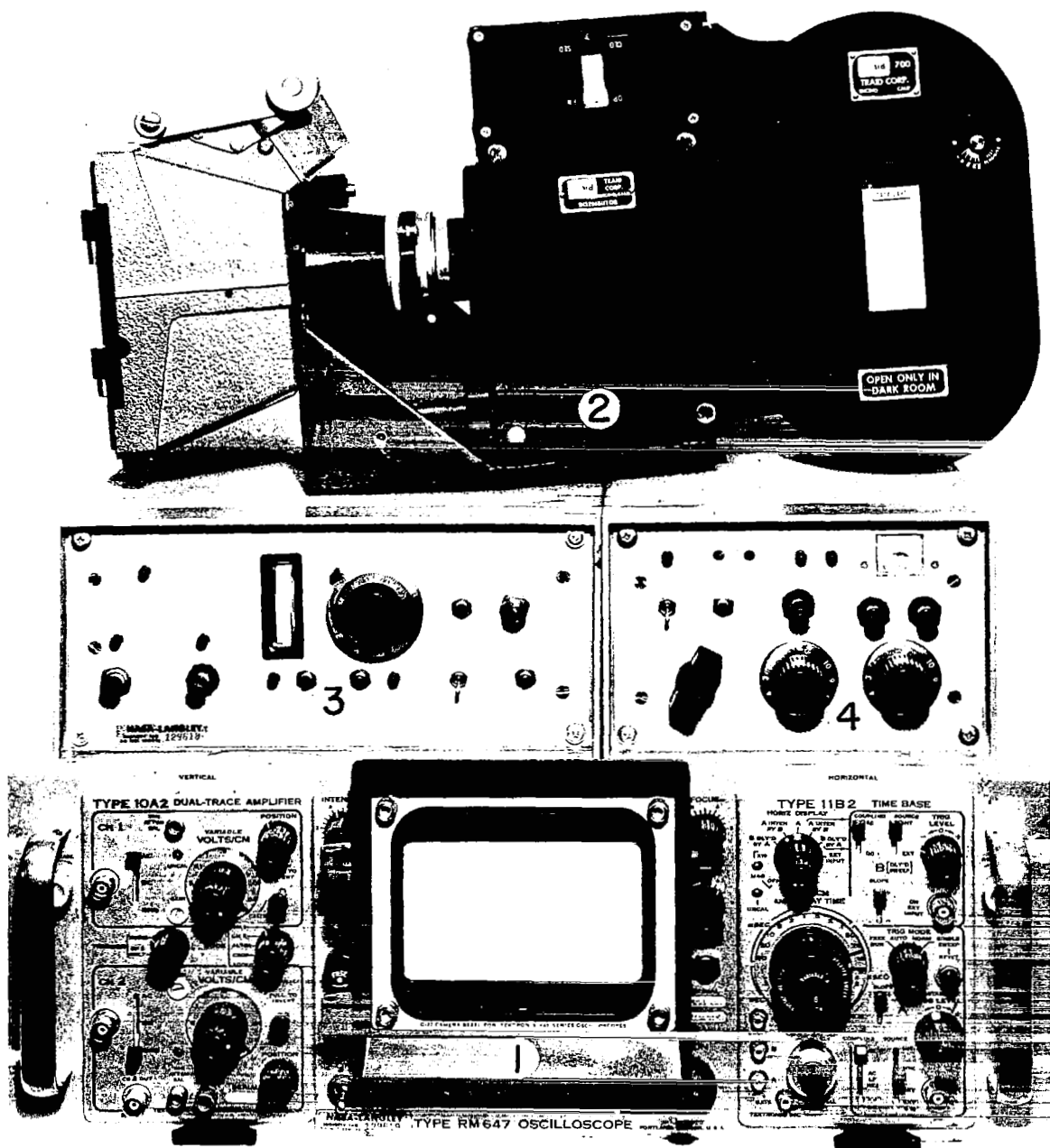
| ① | Oscilloscope | ③ | Transmitter control box |
| ② | 35 mm camera | ④ | Receiver control box |

Figure 6.- Display and recording subsystem and system controls.   L-67-6366.1
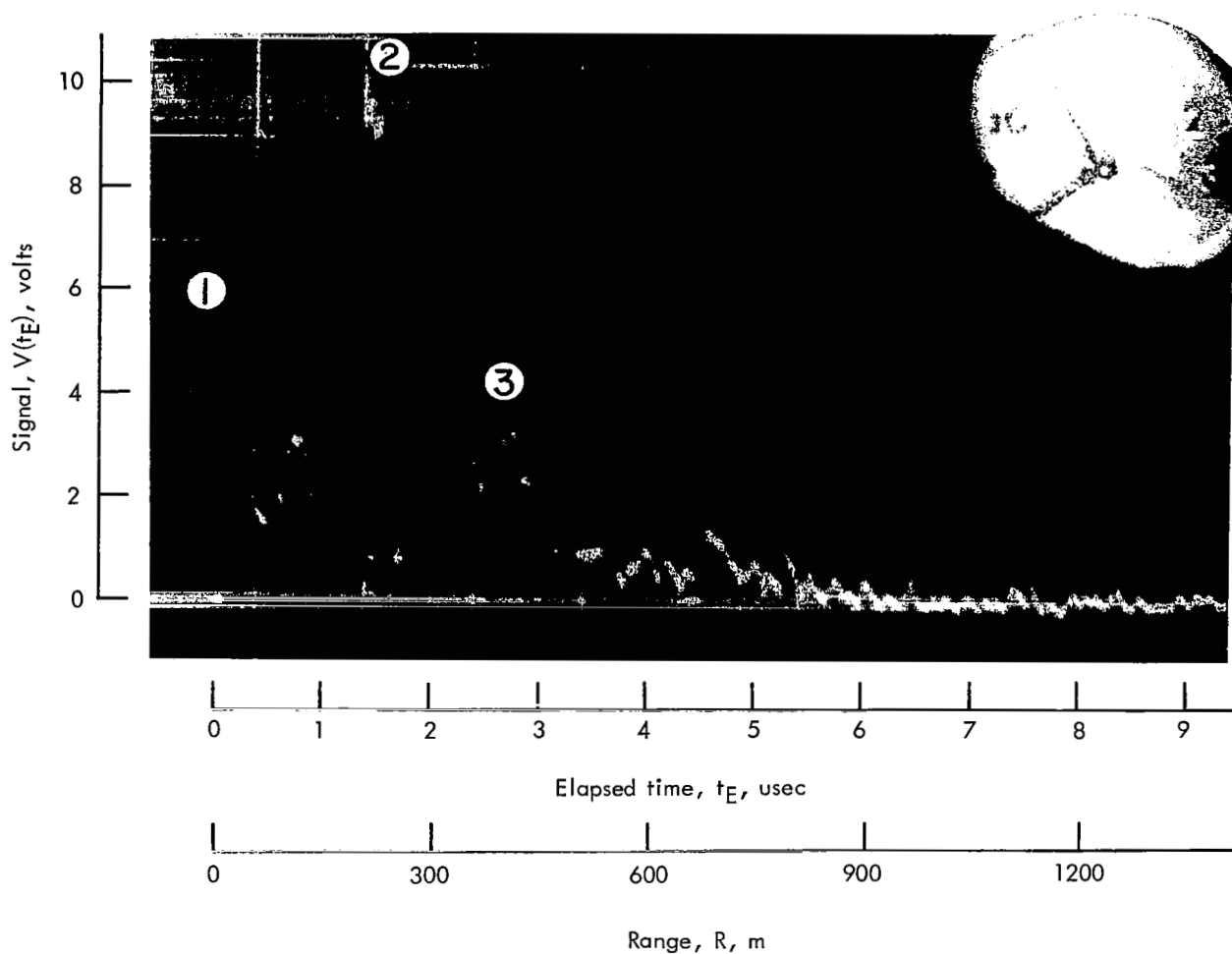
① Peak of the integrated output of the photodiode, which indicates total energy output of the laser

② Crossover of the transmitted beam and the field of view of the receiver

③ The normal R^{-2} falloff of the atmospheric return.

Figure 7.- Oscilloscope trace taken with airplane flying in level flight at an altitude of 0.31 kilometer over Williamsburg, Virginia (lat. 37°17' N, long. 76°45' W).
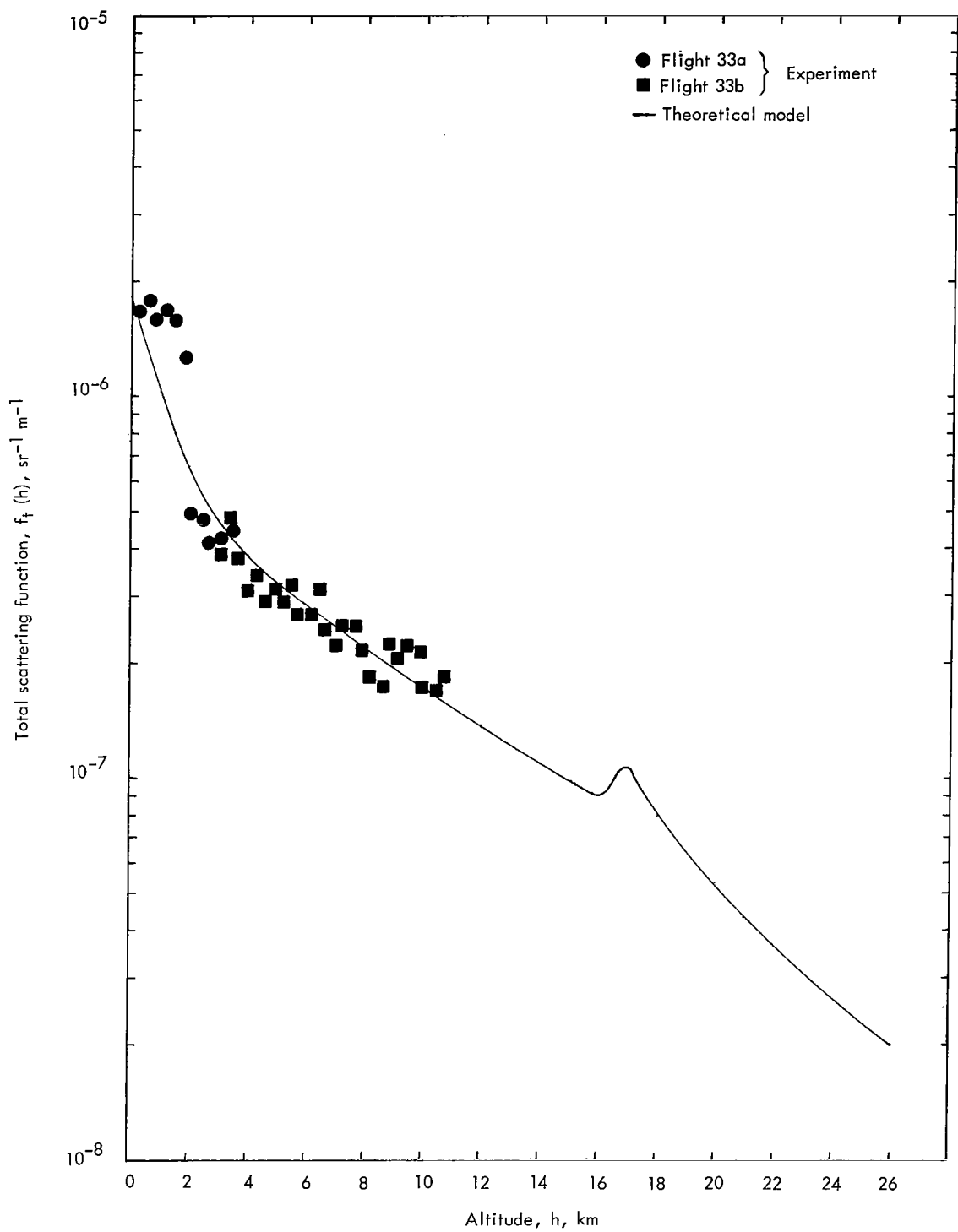
Figure 8.- Comparison of experimental results obtained on the night of March 9, 1967, over Williamsburg, Virginia (lat. 37°17' N, long. 76°45' W), with the theoretical model.
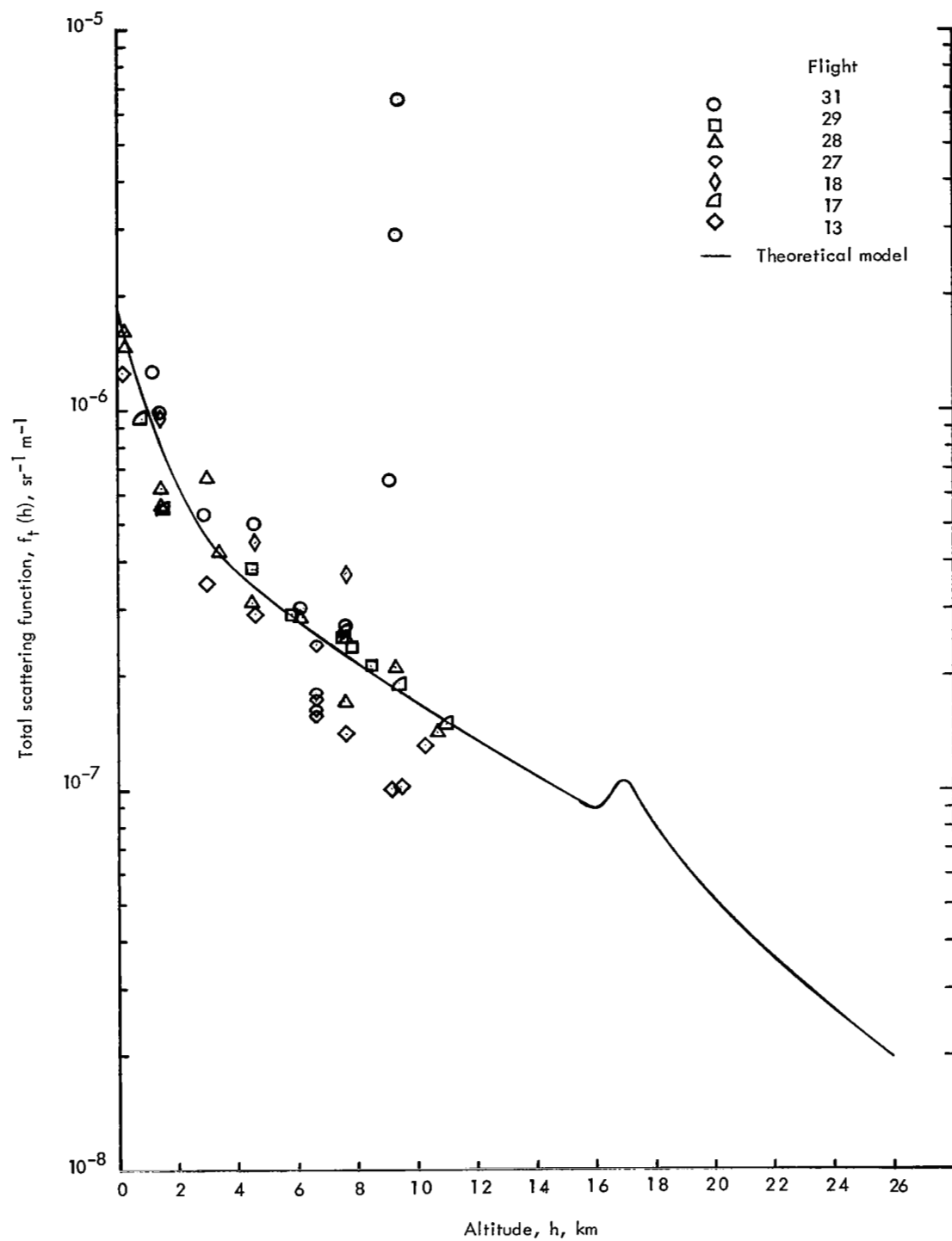
Figure 9.- Composite of experimental data taken from March 1966 to April 1967 over Williamsburg, Virginia and the local coastal region of the Atlantic Ocean.

41
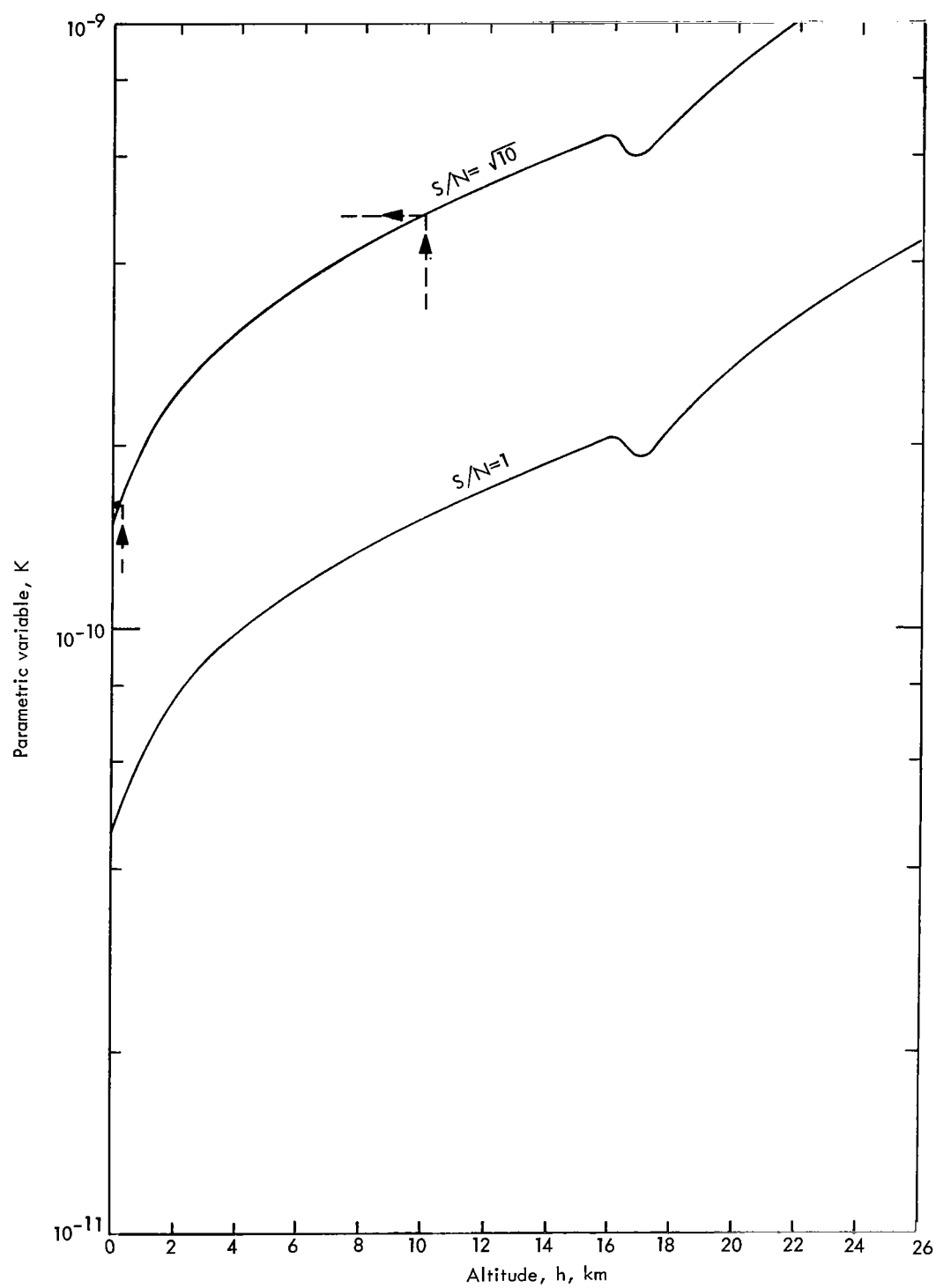
Figure 10.- Total signal detectability curves for $S/N = 1$ and $\sqrt{10}$.
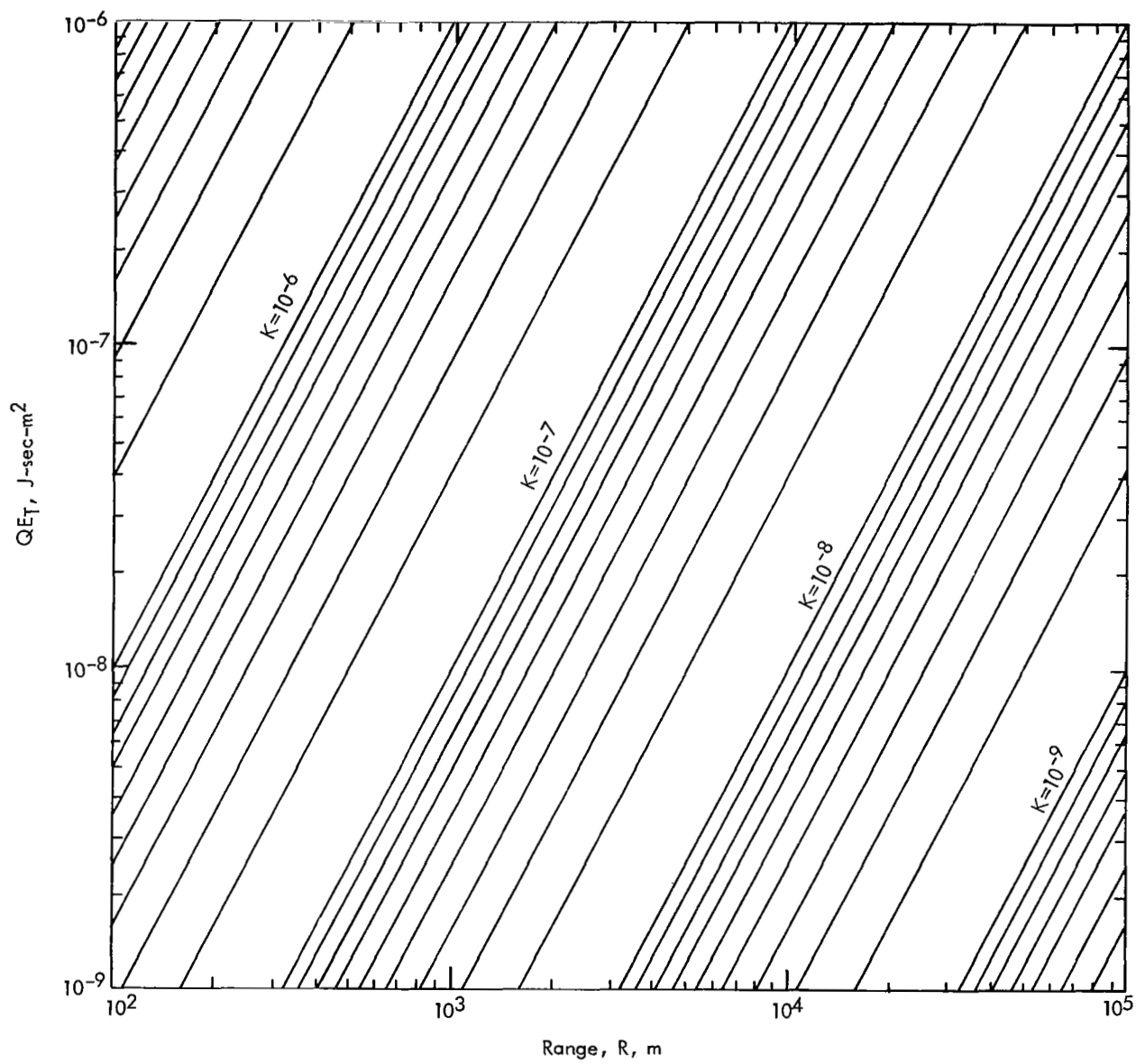
(a) $QE_T = 10^{-9}$ to 10^{-6}.

Figure 11.- Curves relating QE_T with R for constant values of K.
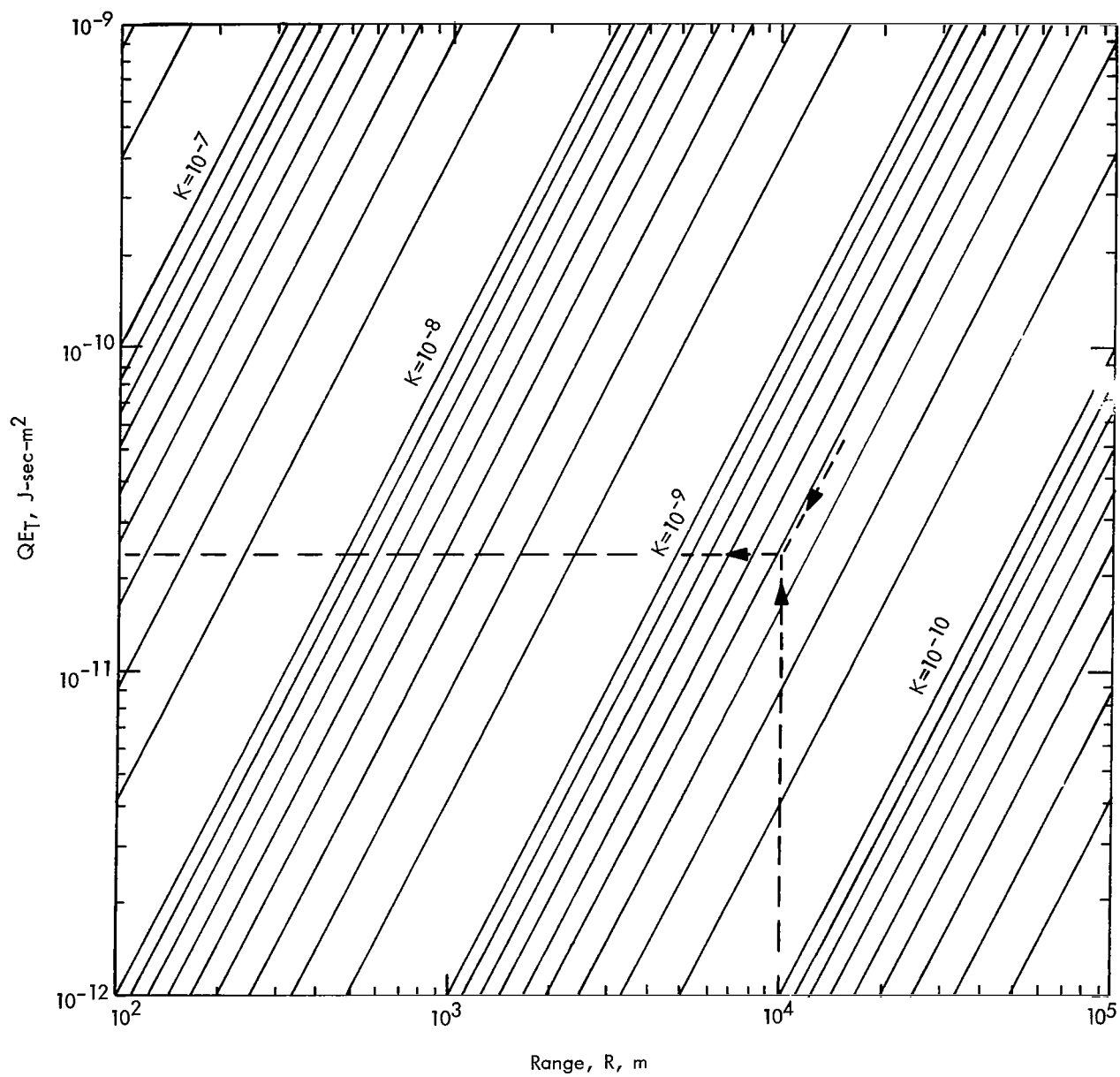
(b) $QE_T = 10^{-9}$ to 10^{-12}.

Figure 11.- Continued.
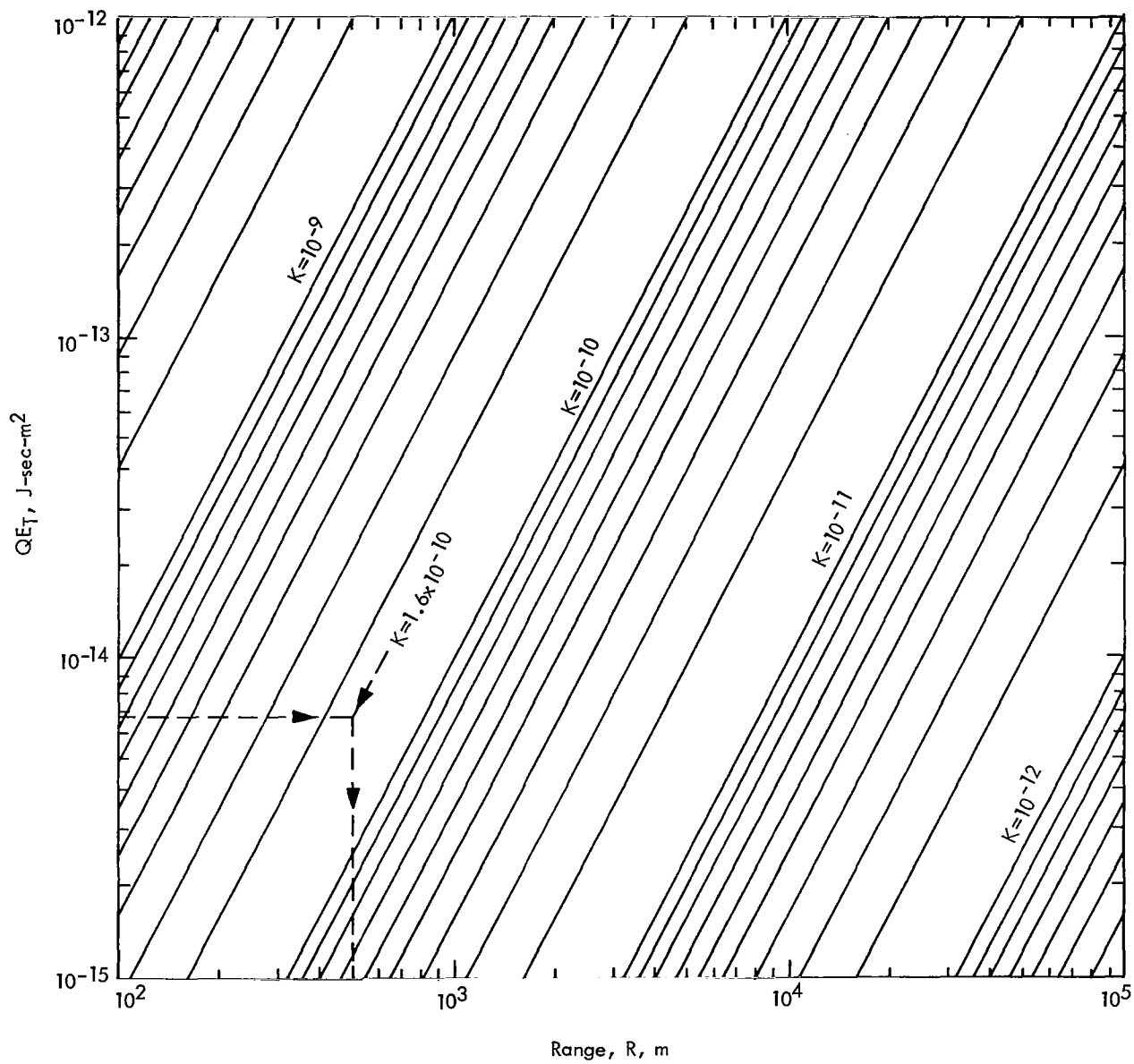
(c) $QE_T = 10^{-12}$ to 10^{-15}.

Figure 11.- Concluded.
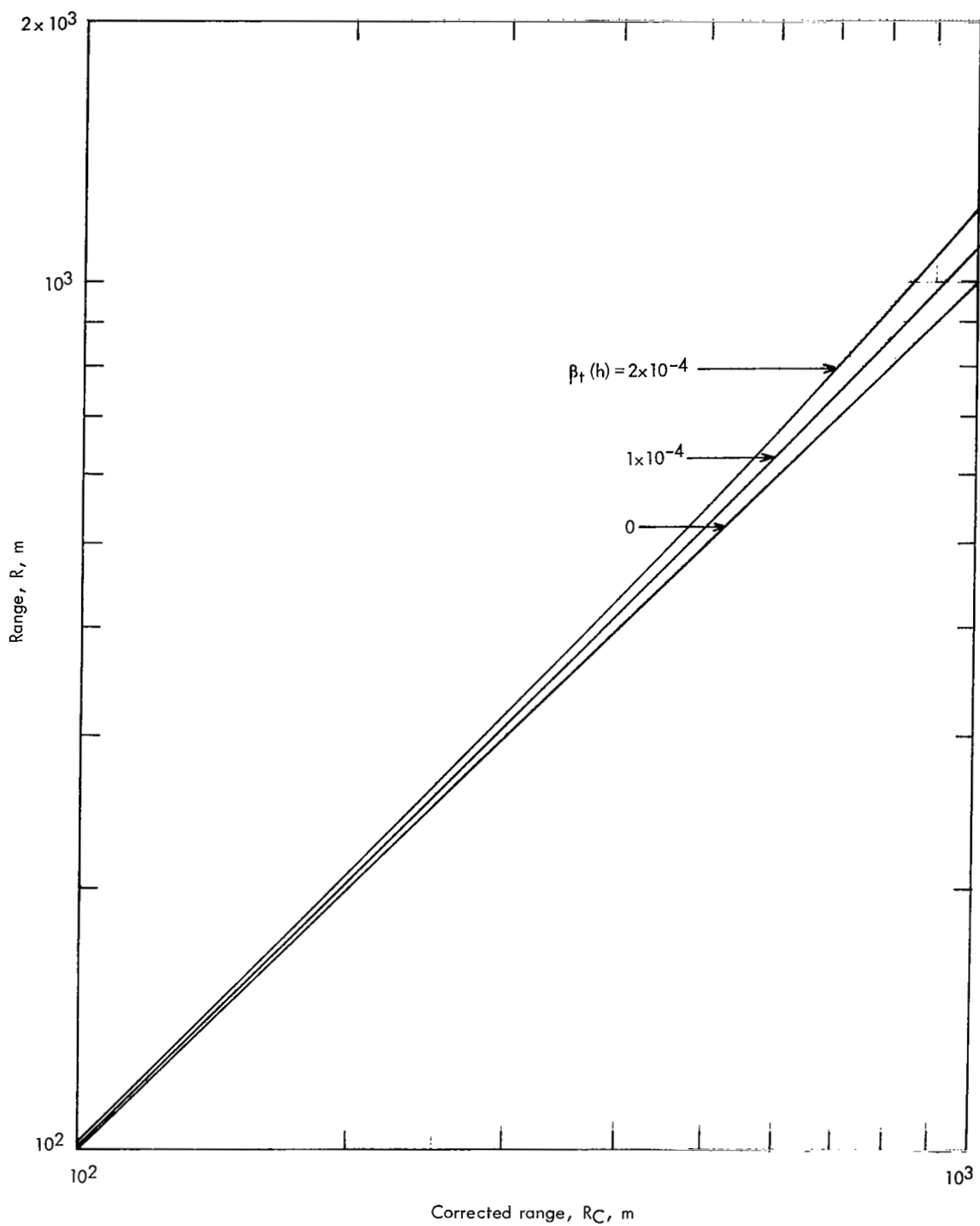
(a) $R_C = 10^2$ to 10^3 meters.

Figure 12.- Predicted range R as a function of corrected range R_C for constant values of $\beta_t(h)$.
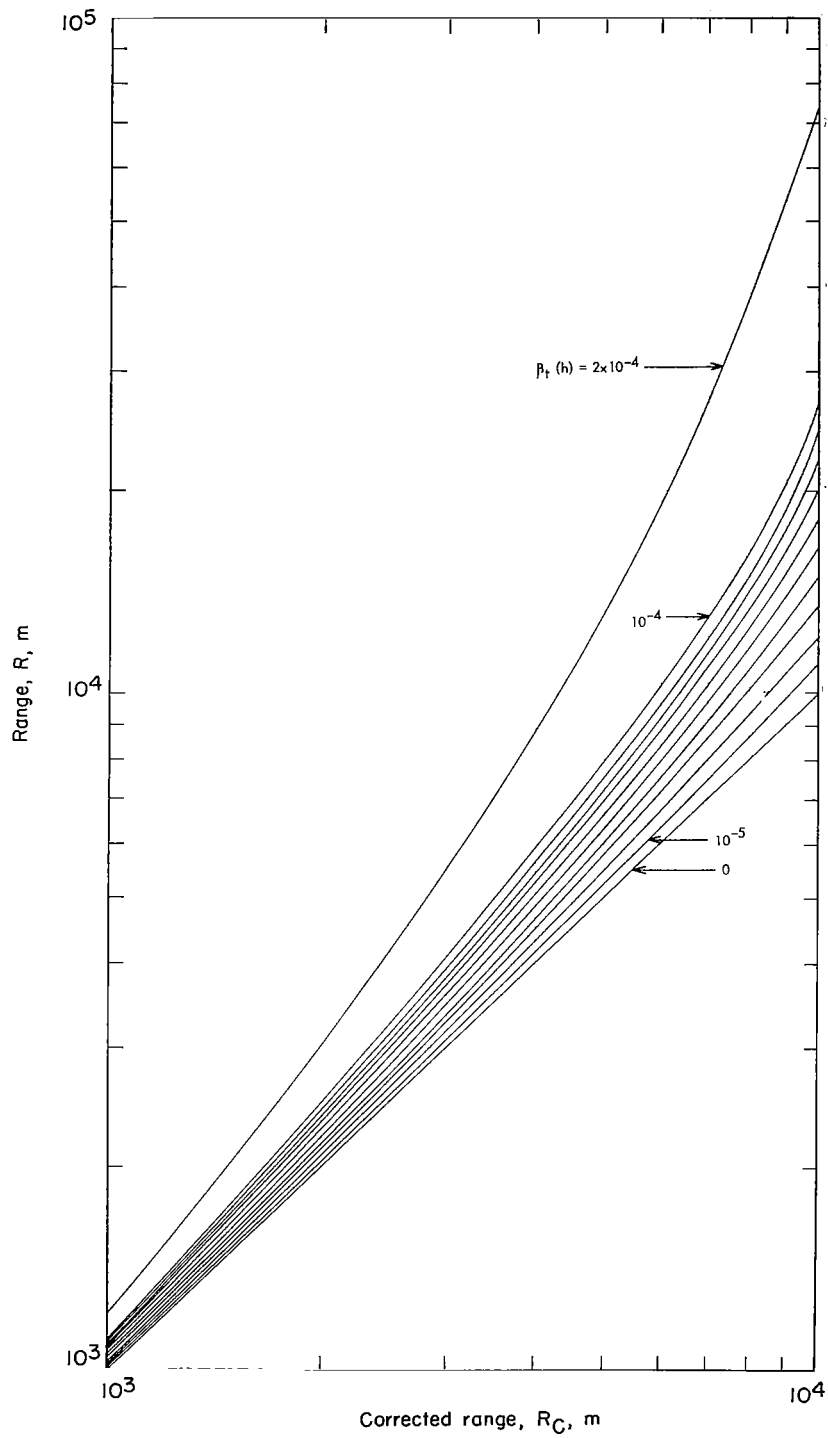
(b) $R_C = 10^3$ to 10^4 meters

Figure 12.- Continued.
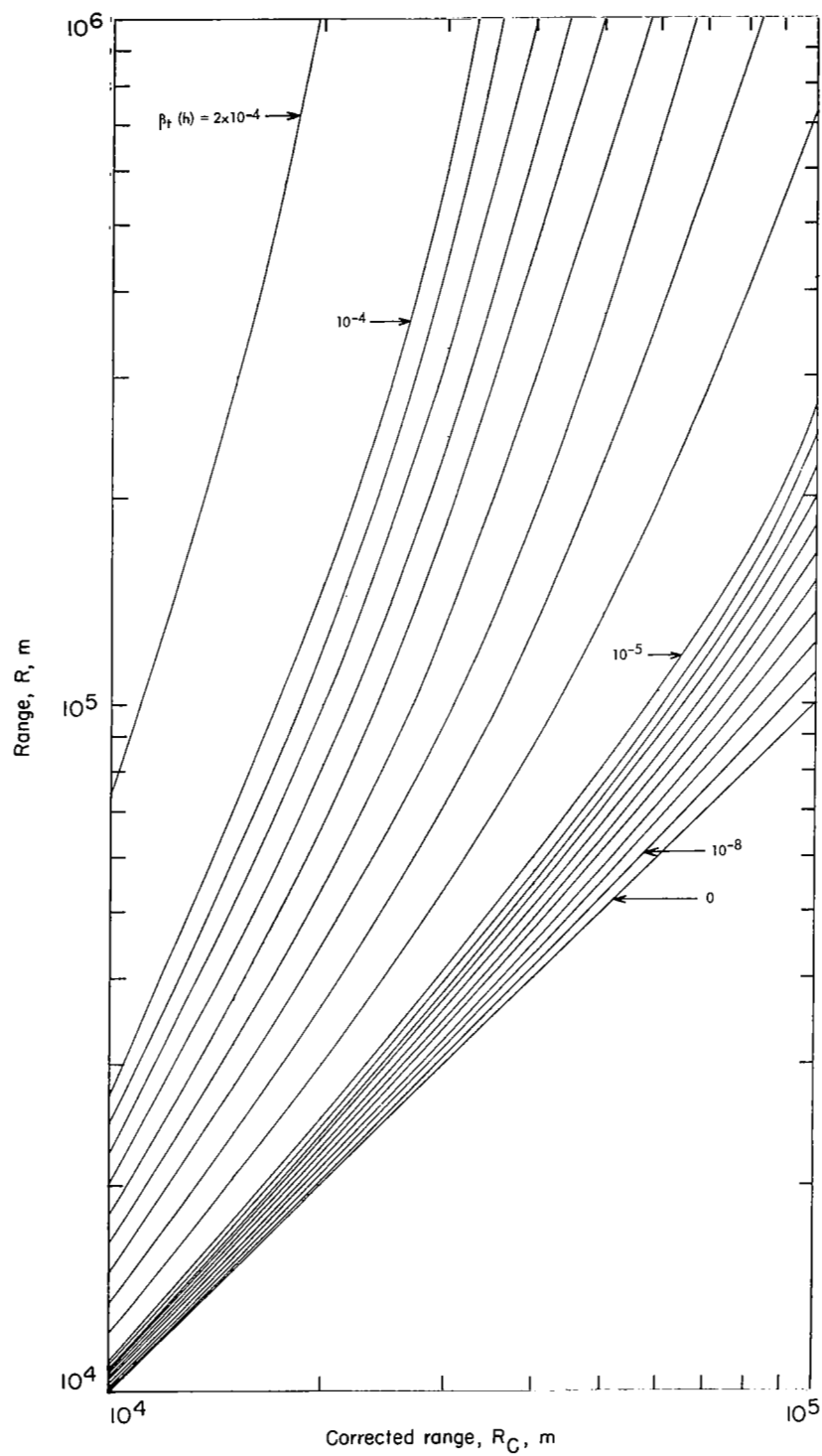
(c) $R_C = 10^4$ to 10^5 meters.

Figure 12.- Concluded.
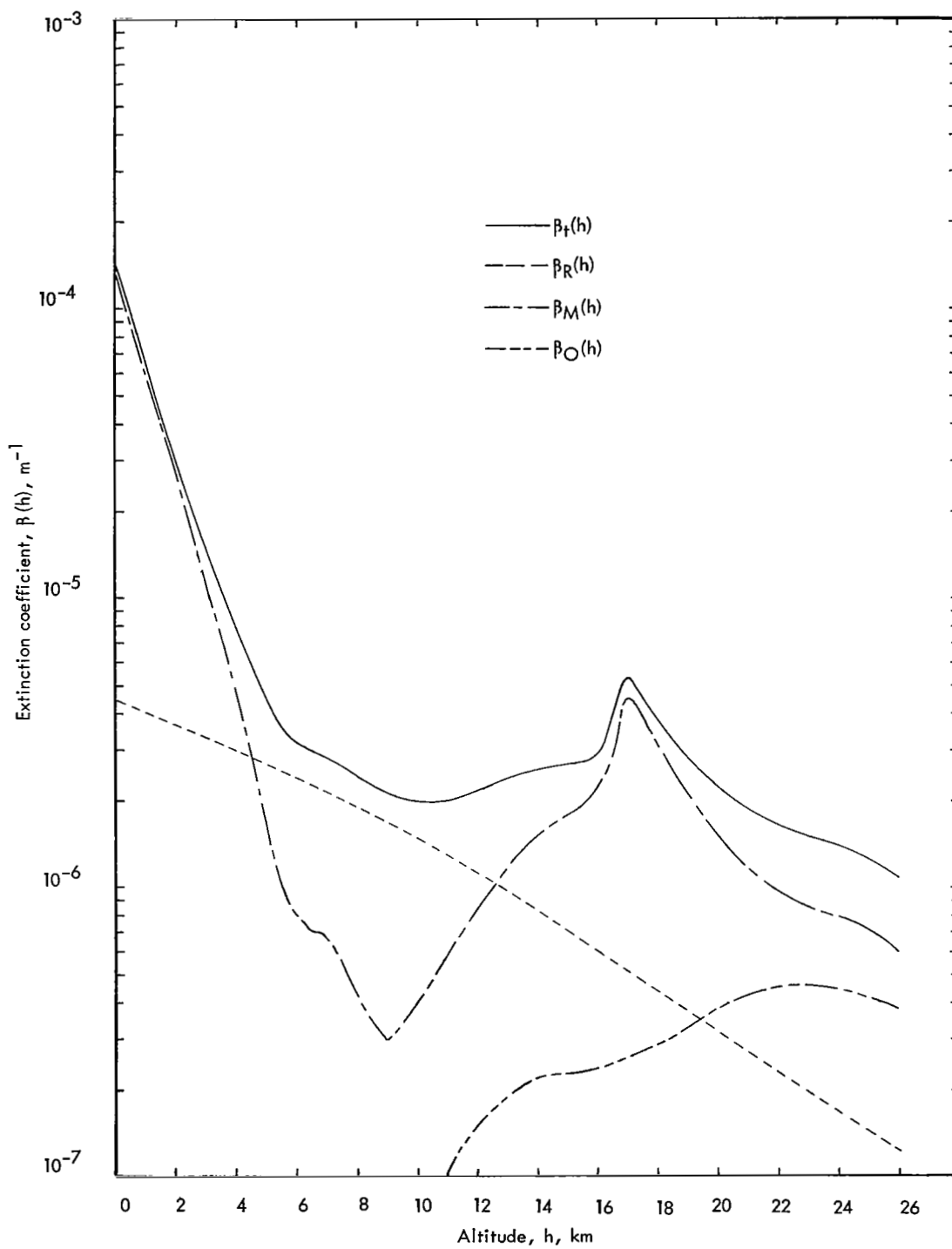
Figure 13.- Extinction coefficient for the lower atmosphere.
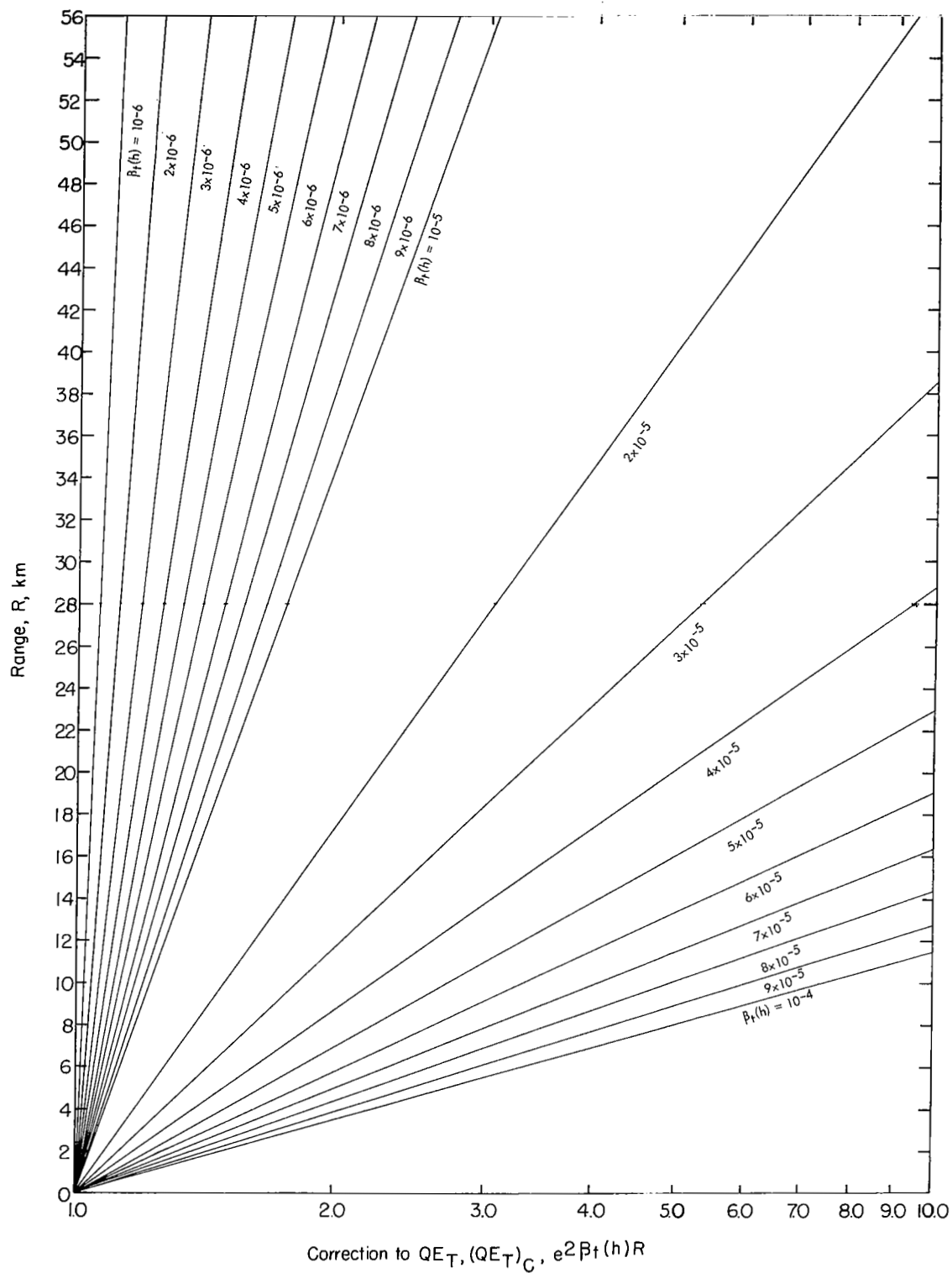
Figure 14.- Attenuation correction to QE_T for a given R and $\beta_t(h)$.
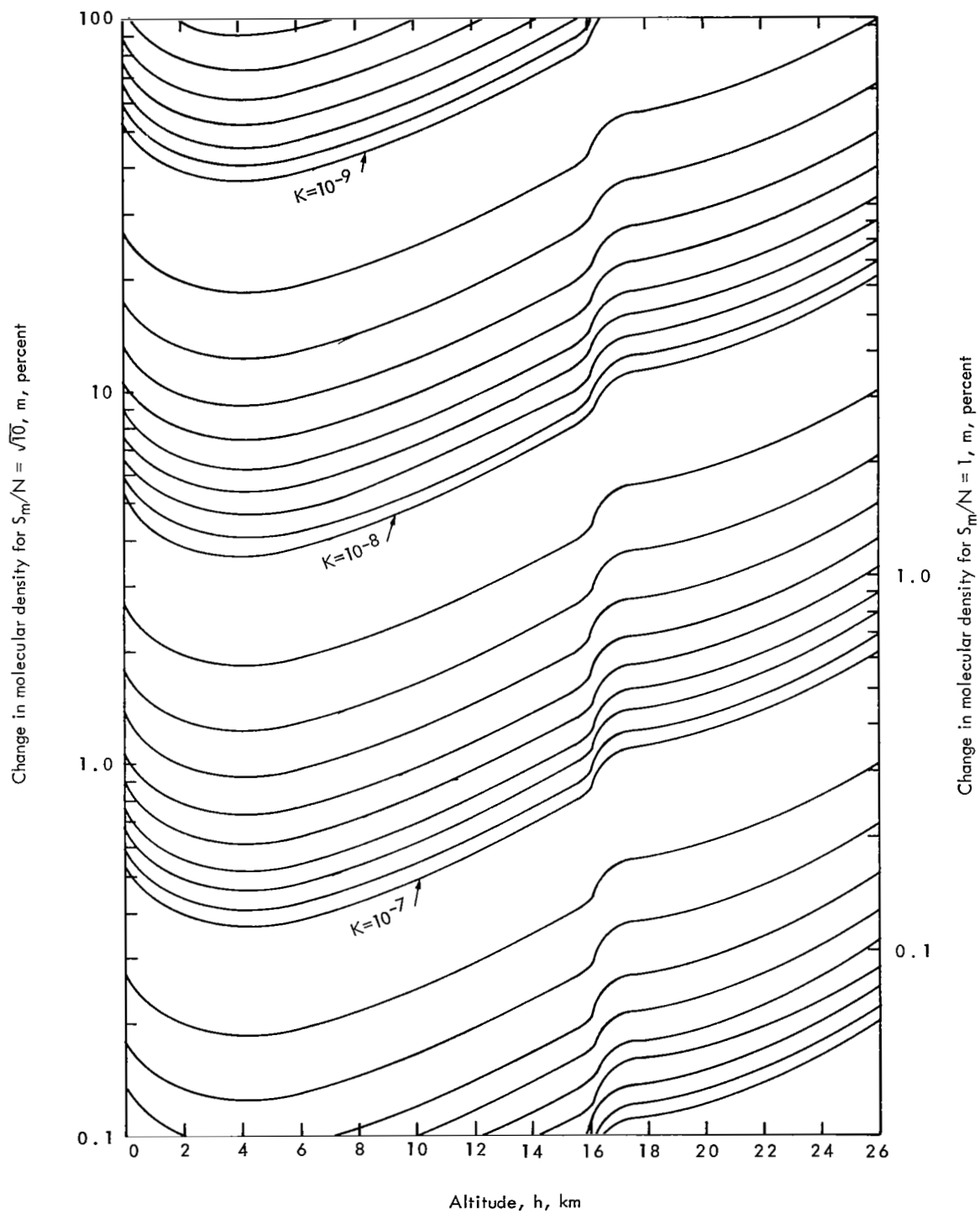
Figure 15.- Molecular change detectability curves for $S_m/N = 1$ and $\sqrt{10}$.
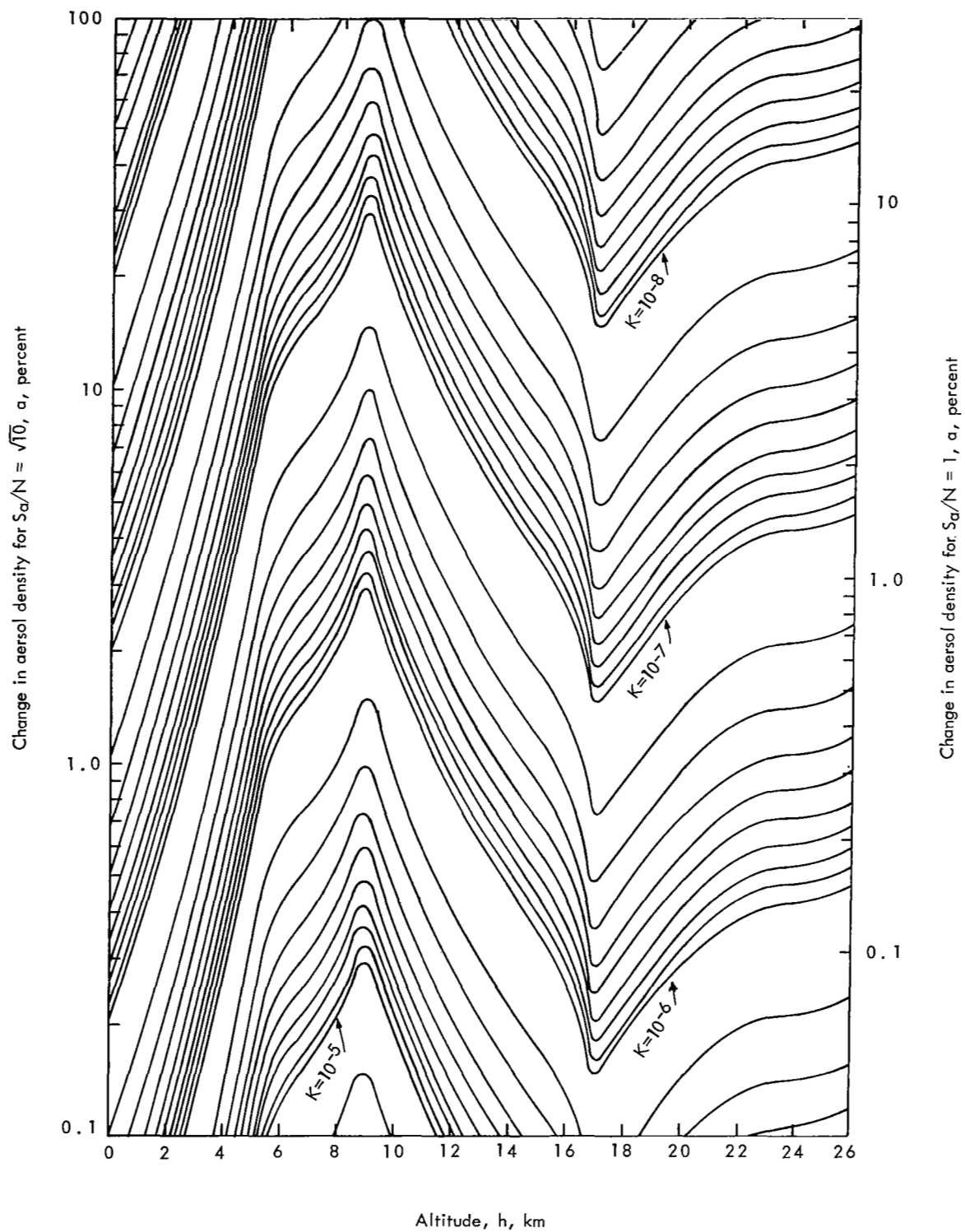
Figure 16.- Aerosol change detectability curves for $S_a/N = 1$ and $\sqrt{10}$.
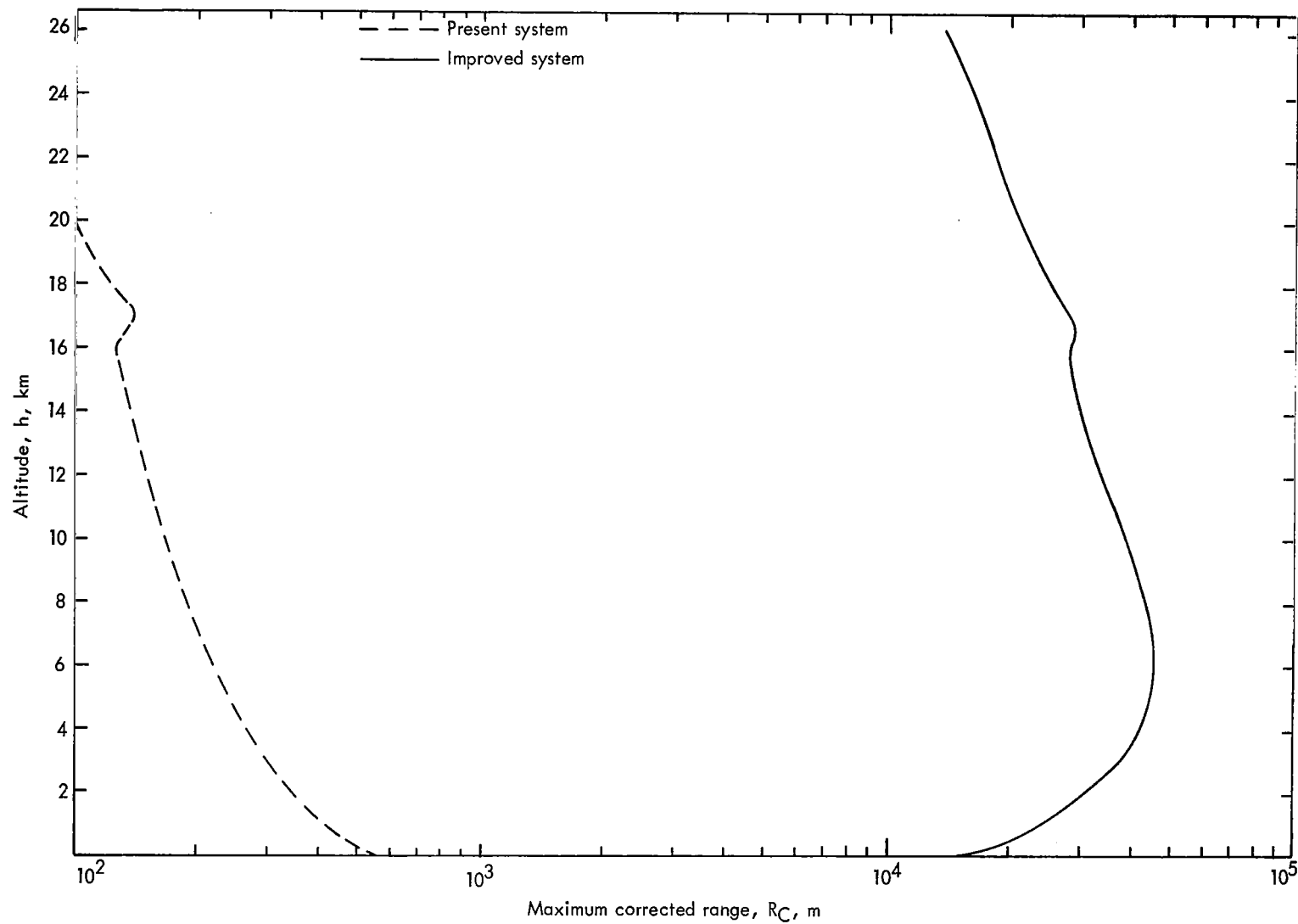
Figure 17.- A comparison of the present and improved system's limit of signal detectability with $S/N = \sqrt{10}$.
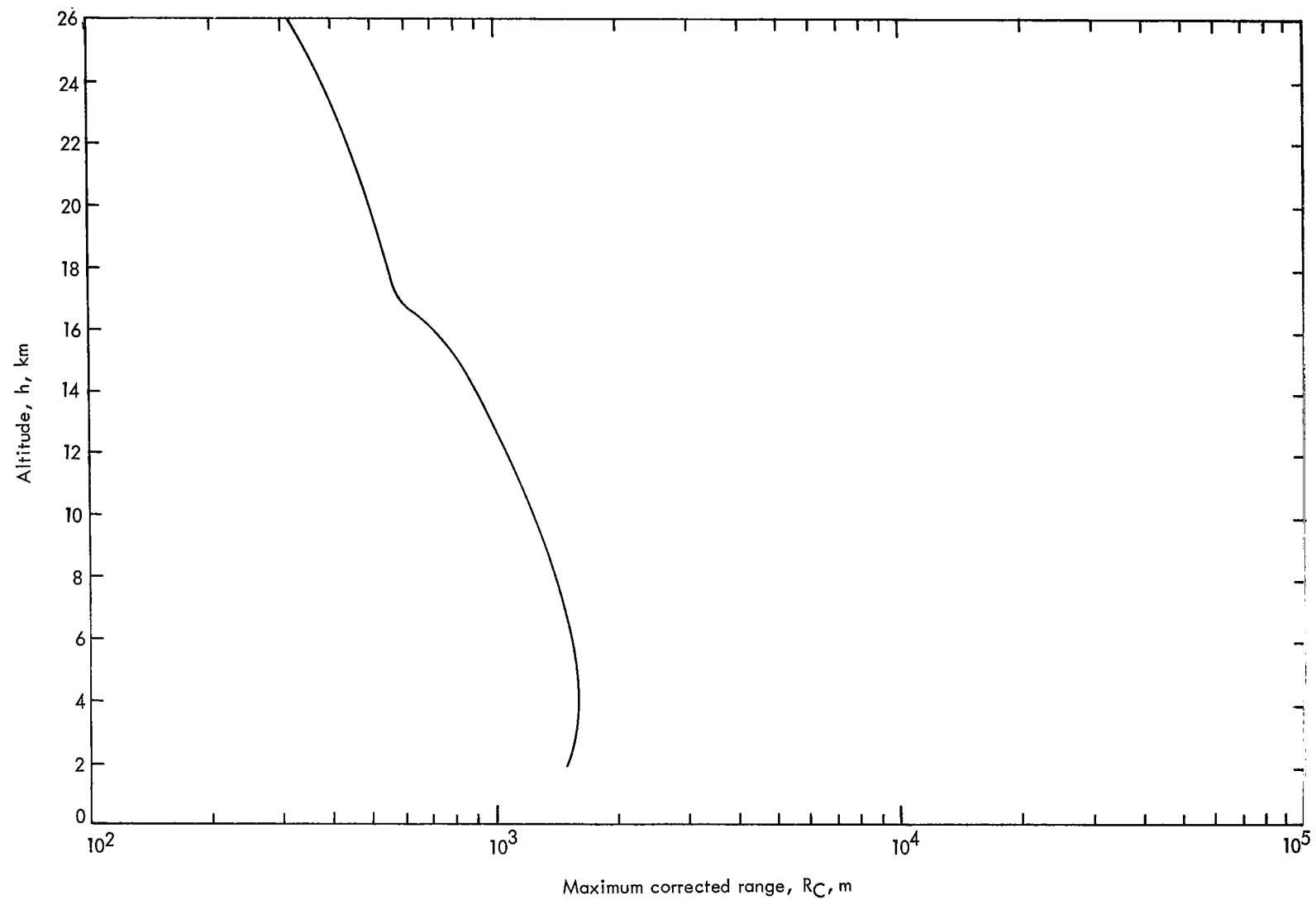
Figure 18.- Capability of the improved system to detect a 1-percent change in molecular density with $S_m/N = 1$.
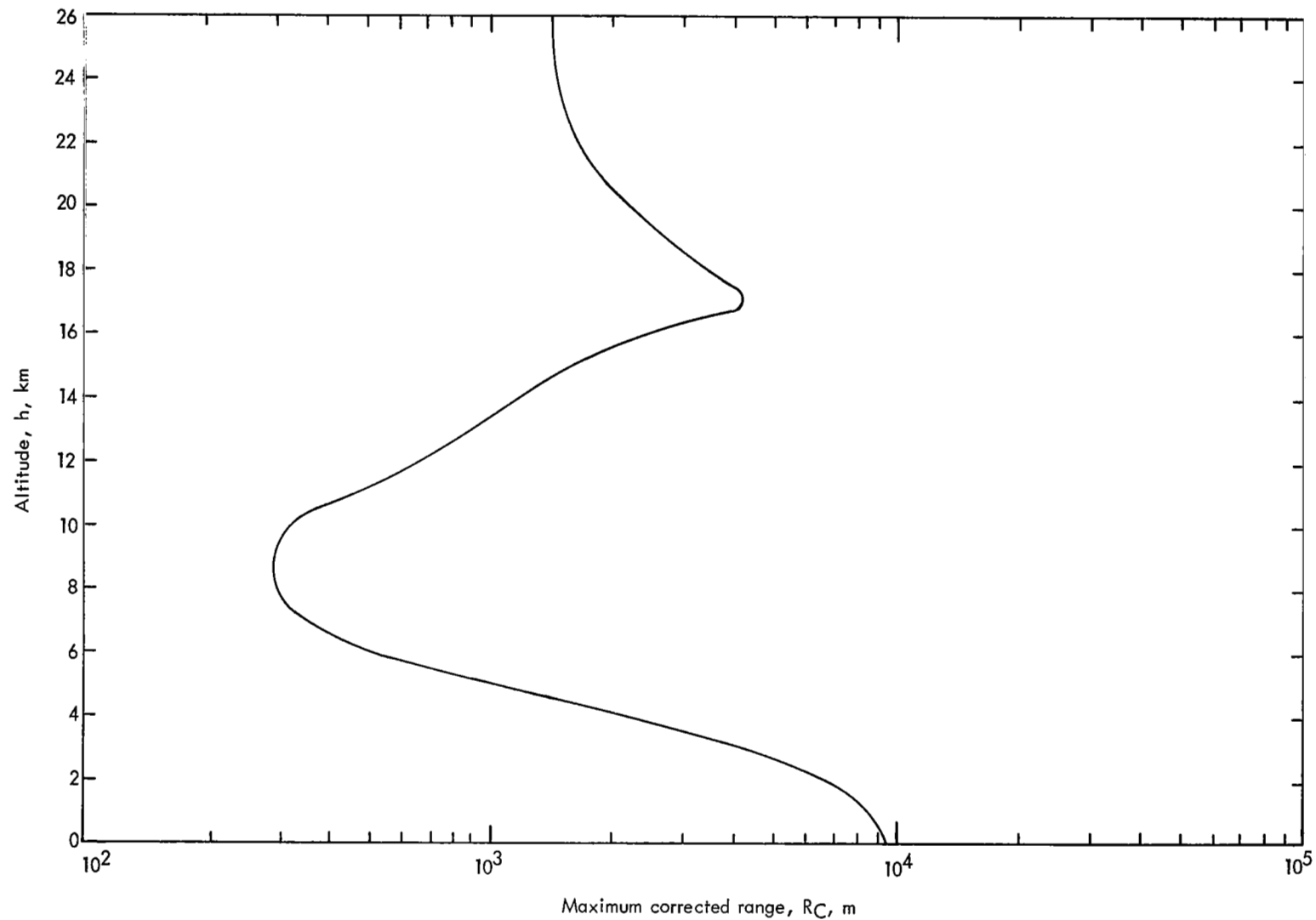
Figure 19.- Capability of the improved system to detect a 10-percent change in aerosol density with $S_a/N = 1$.
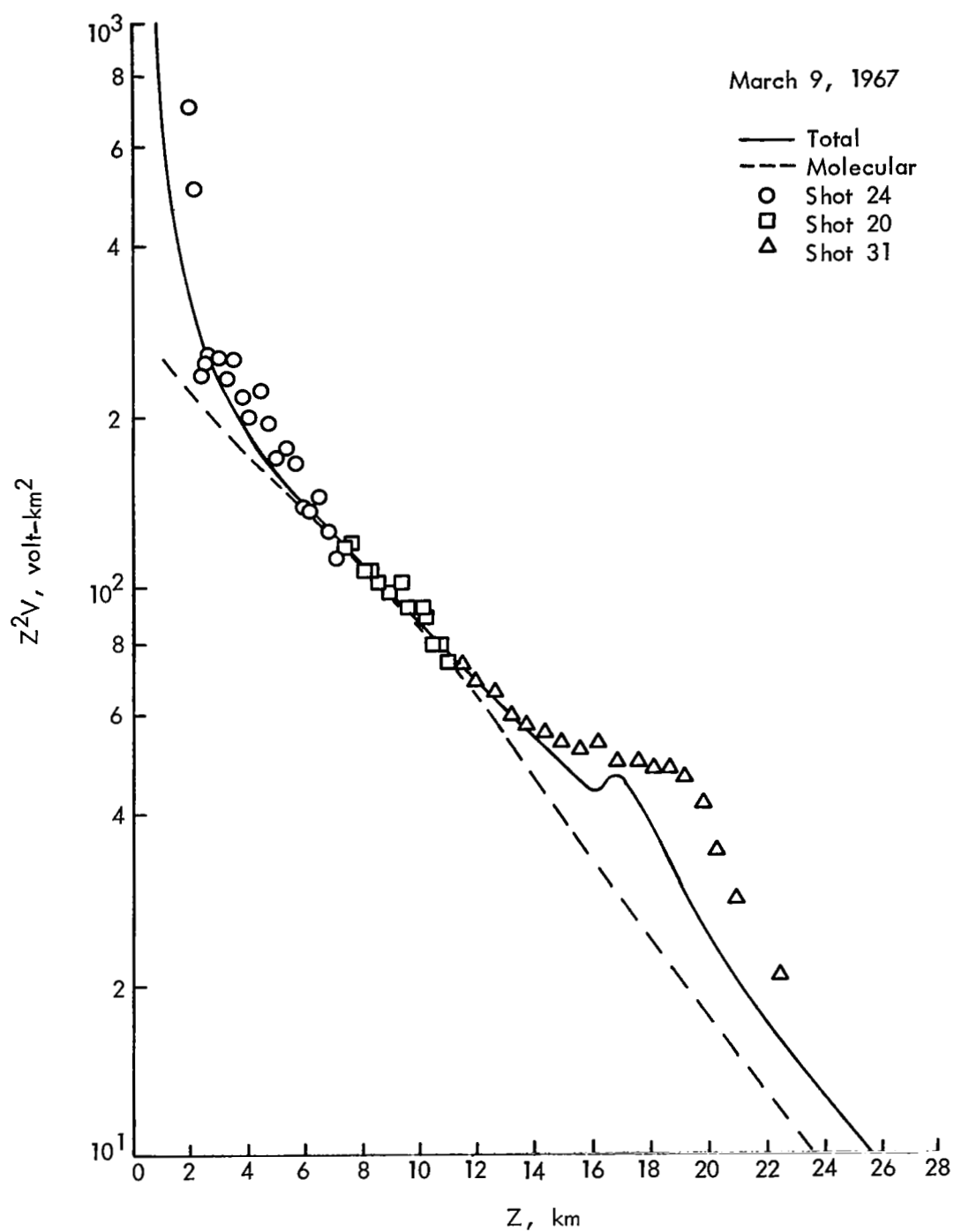
Figure 20.- Data taken from reference 29 in which experimental scattering data are compared with theoretical predictions. Z^2V (in the notation of ref. 29) is the product of signal voltage times the square of the altitude and is approximately proportional to $f_t(h)$ of the present paper.

"*The aeronautical and space activities of the United States shall be conducted so as to contribute . . . to the expansion of human knowledge of phenomena in the atmosphere and space. The Administration shall provide for the widest practicable and appropriate dissemination of information concerning its activities and the results thereof.*"

— NATIONAL AERONAUTICS AND SPACE ACT OF 1958

NASA SCIENTIFIC AND TECHNICAL PUBLICATIONS

TECHNICAL REPORTS: Scientific and technical information considered important, complete, and a lasting contribution to existing knowledge.

TECHNICAL NOTES: Information less broad in scope but nevertheless of importance as a contribution to existing knowledge.

TECHNICAL MEMORANDUMS: Information receiving limited distribution because of preliminary data, security classification, or other reasons.

CONTRACTOR REPORTS: Scientific and technical information generated under a NASA contract or grant and considered an important contribution to existing knowledge.

TECHNICAL TRANSLATIONS: Information published in a foreign language considered to merit NASA distribution in English.

SPECIAL PUBLICATIONS: Information derived from or of value to NASA activities. Publications include conference proceedings, monographs, data compilations, handbooks, sourcebooks, and special bibliographies.

TECHNOLOGY UTILIZATION PUBLICATIONS: Information on technology used by NASA that may be of particular interest in commercial and other non-aerospace applications. Publications include Tech Briefs, Technology Utilization Reports and Notes, and Technology Surveys.

Details on the availability of these publications may be obtained from:

SCIENTIFIC AND TECHNICAL INFORMATION DIVISION

NATIONAL AERONAUTICS AND SPACE ADMINISTRATION
Washington, D.C. 20546